REPORT DOCUMENTATION PAGE

1. REPORT DATE (DD-MM-YYYY)	2. REPORT TYPE	3. DATES COVERED (From - To)
20-07-09	FINAL REPORT	1 APR 06 - 31 MAR 09

4. TITLE AND SUBTITLE

PIEZOELECTRIC CERAMICS
FOR HIGH TEMPERATURE ACTUATORS

5a. CONTRACT NUMBER

5b. GRANT NUMBER

FA9550-06-1-0260

5c. PROGRAM ELEMENT NUMBER

6. AUTHOR(S)

Sayir, Ali
Sehirlioglu, Alp

5d. PROJECT NUMBER

5e. TASK NUMBER

5f. WORK UNIT NUMBER

7. PERFORMING ORGANIZATION NAME(S) AND ADDRESS(ES)

CASE WESTERN RESERVE UNIVERSITY
10900 Euclid Avenue
Cleveland, OH 44106

8. PERFORMING ORGANIZATION REPORT NUMBER

9. SPONSORING/MONITORING AGENCY NAME(S) AND ADDRESS(ES)

AFOSR
875 N. Randolph St.
Suite 325
Arlington, VA 22203

10. SPONSOR/MONITOR'S ACRONYM(S)

AFOSR

11. SPONSOR/MONITOR'S REPORT NUMBER(S)

AFRL-OSR-VA-TR-2012-0406

12. DISTRIBUTION/AVAILABILITY STATEMENT

A

13. SUPPLEMENTARY NOTES

14. ABSTRACT

High temperature piezoelectrics have been developed to expand the operating conditions of actuators for fuel modulation and dampening of high temperature structural parts. Development of high temperature piezoelectric ceramics will increase the efficiency of engines, decrease emissions and improve the life of structural components in aerospace and aeronautical applications that are strongly relevant to the Department of Defense missions. Actuators require application of electric field to obtain displacement that can be used to move loads, block or disturb flow at high frequencies and create acoustic and ultrasonic waves. Ceramics are stable at high temperatures, however their conductivity starts to increase.

15. SUBJECT TERMS

16. SECURITY CLASSIFICATION OF:			17. LIMITATION OF ABSTRACT	18. NUMBER OF PAGES	19a. NAME OF RESPONSIBLE PERSON
a. REPORT	b. ABSTRACT	c. THIS PAGE		39	Dr. Joan Fuller

19b. TELEPHONE NUMBER (Include area code)
703-696-8457

Final Report:

PIEZOELECTRIC CERAMICS
FOR HIGH TEMPERATURE ACTUATORS
FA9550-06-1-0260

Submitted in response to
Air Force Office Scientific Research (AFOSR)

Attention: Dr. Joan Fuller
Deputy Director

Directorate of Aerospace, Chemistry and Material Sciences
Air Force Office of Scientific Research
875 North Randolph Street
Suite 325, Room 3112
Arlington, Virginia 22203
Phone: (703)696-7236
Fax: (703)696-8451

Lead Organization:

CASE WESTERN RESERVE UNIVERSITY

PI-Ali Sayir
Research Associate Professor

Technical Summary

High Temperature Piezoelectric Ceramics for Actuator Applications

PI- Ali Sayir and Co-Investigator Alp Sehirlioglu

High temperature piezoelectrics have been developed to expand the operating conditions of actuators for fuel modulation and dampening of high temperature structural parts. Development of high temperature piezoelectric ceramics will increase the efficiency of engines, decrease emissions and improve the life of structural components in aerospace and aeronautical applications that are strongly relevant to the Department of Defense missions. Actuators require application of electric field to obtain displacement that can be used to move loads, block or disturb flow at high frequencies and create acoustic and ultrasonic waves. Ceramics are stable at high temperatures, however their conductivity starts to increase. In addition, to be operational at high temperature these materials still have to be able to induce large displacements. Hence, this project had three main objectives; (i) increased Curie temperature, (ii) increased resistivity at elevated temperatures and (iii) enhanced piezoelectric activity.

The focus of this research has been science-based development of $BiScO_3$-$PbTiO_3$ based ceramics to produce high temperature piezoelectrics. Two approaches were taken to enhance these ceramics; (i) structural engineering and (ii) compositional engineering. The scientific approach used in this project involved high levels of complexity. The significance and expected impact expected to be long lasting since this project demonstrated pathway to engineer seemingly opposing piezoelectric properties. As a result of this complex engineering, we demonstrated the following piezoelectric properties;

1. Increase the operating temperature by 90 ^{o}C in comparison to state of the art PZT Type II
2. Obtain ceramics with $d_{33} \approx 500$ pC/N
3. Doubled the electrical hardness in comparison to PZT Type II.

We submitted six papers to be published in high quality research journals such as Journal of Applied Physics, Journal of the American Ceramic Society and Journal of Electroceramics. Two papers have already been published and remaining four papers are submitted for publication and in review. In addition, we presented five invited seminars, two invited presentations and four oral presentations in international meetings, academia and government laboratories.

Table of Contents

List of Figures:

List of Tables:

High Temperature Piezoelectric Ceramics for Actuator Applications

I.   Background:

High-temperature piezoelectric materials are sought for aeronautic applications to improve efficiency, reduce emissions, and noise abatement. Piezoelectric actuators for active combustion control mitigates thermo-acoustic instabilities and/ or provide gas flow control to improve mixing characteristics by pulsed air injection to reduce NO_x emission and improve engine efficiency.[1] Synthetic jets for active flow control mitigates boundary layer separation at the blade surface, reduce tip losses, and reduces noise. Active structural control to minimize the blade vibration will reduce stress, increase safety margins, and extend life. Currently, there are no piezoelectric actuators available that can provide enough displacement and force at temperatures exceeding 200^0C, which is the temperature region of interest for aeronautic applications.

Piezoelectricity can be defined as stress (σ) induced electrical displacement (D) (direct effect, Eqn. 1) or electric field (E) induced strain (ε)(converse effect, Eqn. 2).

$$D_i = d_{ijk}\sigma_{jk} \qquad Eqn. 1$$

$$\varepsilon_{jk} = d_{ijk}E_i \qquad Eqn.2$$

The former effect is used in applications such as pressure sensors, accelerometers, energy harvesting and passive damping, while the latter is used in the actuators. Several applications such as medical ultrasound and active dampers utilize both effects.

Large piezoelectric displacements are obtained from material systems that have a morphotropic phase boundary (MPB), such as $PbZrO_3$–$PbTiO_3$ (PZT) and $Pb(Mg_{1/3}Nb_{2/3})O_3$–$PbTiO_3$ (PMN–PT).[3–5] The piezoelectric strain coefficient, d_{ijk}, is enhanced at the MPB region due to coexistence of multiple phases, whose polarization vectors become more readily aligned by an applied electric field. PZT family of ceramic systems that are engineered at MPB region for high-temperature applications have Curie Temperature (T_C)of 350^0C (i.e., Navy Type II). Further limitation for high-temperature applications is due

to increased electrical conductivity. PZT-based piezoelectric ceramics are limited to 200°C due to decreased electrical resistivity and thermal depoling. Thus, main challenges in developing high-temperature piezoelectrics are:

(i) to increase T_c without increasing the temperature-dependent loss tangent (tan δ),

(ii) to demonstrate high-piezoelectric activity,

(iii) to increase the depoling temperature.

New perovskite systems containing bismuth (BiMeO$_3$, Me=metal) in solid solution with PbTiO$_3$ (PT) exhibit high T_c and large piezoelectric coefficients near the MPB.[2–11] The most promising system is (1-x)BiScO$_3$-xPbTiO$_3$ (BS–PT), with its MPB composition at x=0.64–0.65.[12–15] Several studies on compositional B-site doping and single crystal processing showed the potential for this material to be used at high temperatures.[6–11,16–22] However, conductivity at elevated temperatures limited the use of BS-PT ceramics.

II. Results:

We have systematically studied BS-PT system to elucidate the relationship between microstructure, composition and electrical/electromechanical properties. We have successfully increased the resistivity at high temperatures and the depoling temperature. As a result this new family of ceramics is finely tuned for higher temperature actuator application.

Two approaches were taken to achieve the aforementioned goals: (1) Structural Engineering, and (2) Compositional Engineering

1. Structural Engineering:

Electrical and electromechanical properties of piezoelectrics strongly depend on the microstructure of the ceramics. Grain size, shape and orientation can be modified by processing techniques to obtain superior ceramics. As a part of **Task II** in the proposal we have modified the structure of 0.37BiScO$_3$–0.63PbTiO$_3$ ceramics through liquid phase sintering (LPS). The nominal composition was chosen because of its proximity to MPB. The high temperature properties of the liquid phase sintered ceramics are also reported as a part of **Task III**.

Bi_2O_3 and PbO were chosen as the LPS aids. $BiScO_3$–$PbTiO_3$ system consists of Bi and Pb cations, both of which have oxides with high vapor pressures. The melting temperatures for Bi_2O_3 and PbO are 817°C and 866°C, respectively, much lower than the sintering temperature (1100 °C). In addition to modifying the microstructure, compensation by excess Bi_2O_3 and PbO addition and their partitioning in grains and grain boundaries will affect the piezoelectric properties.

The composition 0.37$BiScO_3$-0.63$PbTiO_3$ was prepared by conventional

Fig 1: X-ray diffraction pattern of calcined $BiScO_3$-$PbTiO_3$ powder showing a single perovskite phase (continuous from 10° to 80° C, 0.02° resolution, and 0.8s per step count time).

ceramics processing. Raw powders of PbO, Bi_2O_3, Sc_2O_3, and TiO_2, with purity levels greater than 99.9% were used. The powders were mixed in the stoichiometric amount and ball milled using yttria-stabilized zirconia balls. Milled powders were calcined at 750 °C for 3 hours in air. X-ray analysis showed that a single phase perovskite was obtained after calcination (Fig. 1). Excess PbO and Bi_2O_3 were added to the calcined powder and mixed via ball milling. Dried powders were then uniaxially pressed into pellets with 12.5mm diameter steel die at 150 MPa. To minimize Pb and Bi loss during sintering, pressed pellets were covered with Pb and Bi containing sacrificial powder. A second crucible was placed on the top of the covered pellets and the area between the two crucibles was filled with more sacrificial powder.

Sintering conditions were determined by dilatometric measurements using a Netzsch 402C horizontal dilatometer (Fig. 2). The onset of sintering was around 615 °C for both the nominal composition and the composition with excess Bi_2O_3. Sintering is completed in the 1000 °C-1200 °C range for the nominal composition giving a density of 7.66 g/cc at 1100 °C as measured by N-propanol immersion. A soak time of one hour at 1100 °C resulted in an additional shrinkage of ≈1% (Fig. 2). Above 1280 °C, the sample deformed as the temperature approached the melting temperature.
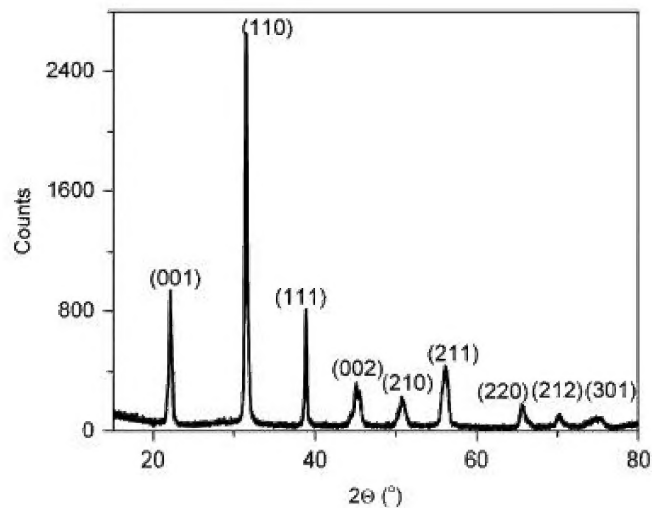
Initial shrinkage for the composition with excess Bi_2O_3 occurred at lower temperature and was complete around 760 °C. This is lower than the melting temperature of Bi_2O_3 ($T_m \approx 817$ °C). Above 1000 °C significant densification occurred as shown in Figure 2. At this stage of sintering densification continued with soaking at a given temperature. For example hold time of one hour at 1100 °C resulted in an additional shrinkage of 9.5%, almost an order of magnitude higher than the nominal composition at the same

Fig. 2: Thermal strain measurements of a $BiScO_3$–$PbTiO_3$ green body as a function of temperature and as a function of time at 1100°C showing the sintering behavior.

temperature (Fig. 2). Density of the specimen with 5% excess Bi_2O_3 sintered at 1100 °C was 7.73 g/cc, that was higher than the nominal composition. Note that there is a slope change around 1230 °C which indicated that the temperature was approaching the melting temperature, consistent with the behavior of the nominal composition. Sintering was performed at 1100 °C for 1hr in air atmosphere. The weight loss during sintering was <2 wt.%, which is similar in value to published data.[3] Sintered pellets were then polished and electroded using silver conducting paste (SPI Supplies).

The Curie temperature was determined using different samples from several batches of 0.37$BiScO_3$-0.63$PbTiO_3$ (37BS-63PT) composition. A reproducible T_c = 430 °C was measured. Curie temperature of 430 °C is lower than published reports ($T_c \approx 445$ °C) for similar compositions by Randall et al.[12,13] To elucidate the difference between our results and literature values, we systematically investigated the compositional and microstructural paradigm. The composition of the calcined powders and sintered pellets were examined by inductively coupled plasma (ICP) analysis and results are summarized in Table I. The compositions of Bi and Pb were the same as starting batched composition, 37% Bi and 63% Pb. The calcined and sintered compositions were same within the experimental error indicating good processing control of the double crucible method. The compositions calculated in reference to Sc content exhibited slightly lower $BiScO_3$/$PbTiO_3$ ratio ($\approx$ 36/64) than calculated in reference to Bi content. Bi/Sc (Pb/Ti) ratio was 0.995 (0.94) and 1.00 (0.96) for calcined and sintered compositions, respectively. This indicated a slight shift in the composition towards $PbTiO_3$ rich side of
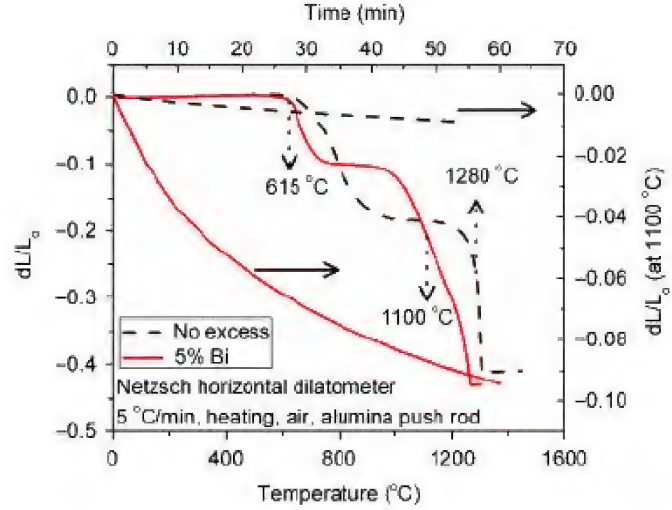
4

the phase diagram, albeit creating Pb deficieny. The ICP results for both calcined powders and sintered pellets revealed that the O/(Bi+Pb) and O/(Sc+Ti) ratios were significantly lower than the expected stochiometric value of three, indicating an oxygen deficient system. To validate the suggestion of oxygen deficiency by ICP, direct measurements of oxygen content were carried out by the Oxygen Determinator. Direct measurements showed a higher amount of oxygen content in both calcined ($O_{2.86}$) and sintered ($O_{2.84}$) specimens compared to ICP calculations. Direct measurements are a more reliable method of measuring the oxygen content ($\pm$ 0.25wt%). In spite of measurement differences, the $0.37BiScO_3$-$0.63PbTiO_3$ (37BS-63PT) system is an oxygen deficient system. This may account for the T_c difference results and Randall et al's[12,13] observations.

Another variation of 37BS-63PT composition with published results was the average grain size. The ceramics processed in this research exhibited an average grain size of 24.8 µm, which was 3.3 times larger than reported by Eitel et al. (7.5 µm) for similar sintering conditions (1100 °C, 45 mins).[3] This indicated that a great degree of grain growth occurred during sintering. The grain growth is strongly dependent on the excess PbO and Bi_2O_3 content and required systematic investigation which is discussed below in separate sections.

i.   **Excess PbO:** Figure 3 shows dielectric constant and loss tangent (tan δ) as a function of temperature for 37BS-63PT with 0%, 2% and 5% excess Pb. The dielectric constant maximizes at the Curie temperature, ranging from 430 to 480 °C with increasing Pb content. The sintered compositions are highly resistive (ρ $\geq 10^{10}$ Ωcm) at low temperatures. Phase angle, tan δ, exhibits a minor dependence on Pb content, e.g., tanδ = 0.02 and 0.05 for 2% and 5% Pb at 55 °C and 10 kHz. The loss tangent was 0.02 for the nominal composition (no excess Pb). At temperatures exceeding 300 °C, tan δ exhibited a more significant dependence on Pb addition (Fig. 3). At 350 °C, the tan δ at 10 kHz was 0.9, 1.3 and 1.7 for 0%, 2% and 5% Pb, respectively.
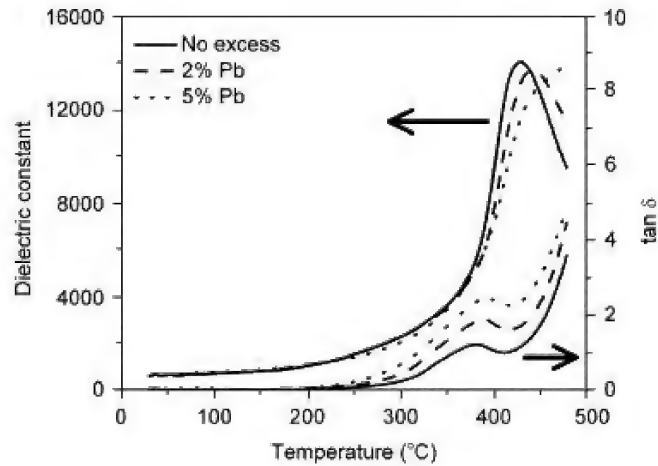

Fig. 3: Dielectric constant and loss tangent (at 10 kHz) as a function of temperature for compositions with 0%, 2%, and 5% excess Pb.

5

Table I. Cation Ratios Measured by ICP for Both Calcined Powders and Sintered Pellet Batched as 0.37BiScO$_3$–0.63PbTiO$_3$

	Bi/(Bi+Pb)	Pb/(Bi+Pb)	Sc/(Sc+Ti)	Ti/(Sc+Ti)	O/(Bi+Pb)	O/(Sc+Ti)	O[1]
Calcined	0.372	0.628	0.358	0.642	2.515	2.411	2.865
Sintered	0.369	0.631	0.360	0.640	2.624	2.563	2.845

Electrical impedance spectroscopy (EIS) was used to characterize electrical conduction. Resistivity is related to grain and grain boundary contributions. Samples were measured from 1 Hz to 1 MHz. EIS spectrum was fitted by mathematical fitting of equivalent electrical circuit elements to separate grain and grain boundary behavior. Grain resistivity and grain dielectric constant were calculated by fitting an equivalent circuit using two sub-circuits in series. The inset in Figure 4 illustrates each sub-circuit using a parallel
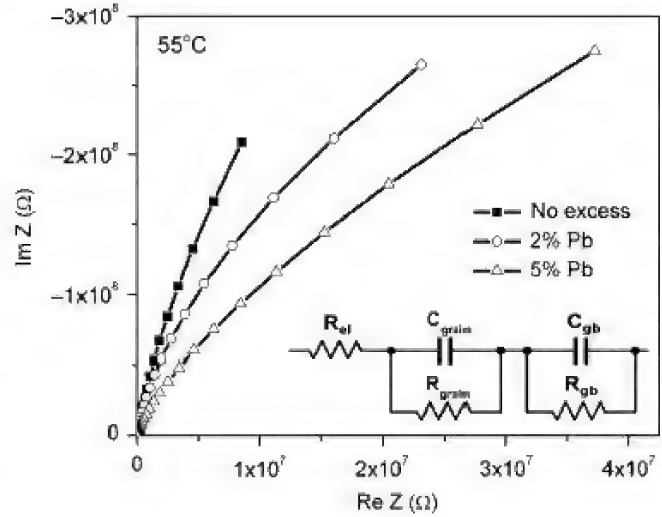

Fig. 4: Impedance results of BiScO$_3$–PbTiO$_3$ with 0%, 2%, and 5% excess Pb at 55°C measured from 1 Hz to 1 MHz. Inset showing the equivalent circuit used for fitting.

circuit containing a constant phase element and resistor to represent electrical behavior. These two sub-circuits corresponded to the grain and the grain boundary response. Calculated electrical properties are presented in Table II. Below 150 °C, there is no relaxation and the grain and grain boundary response are indistinguishable.

The grain resistivity (ρ_{grain}) decreased with excess Pb content. Even at temperatures as low as 55 °C, the effect of excess Pb was significant and grain resistivity decreased from 4.1x10^{10} Ω.cm (0 % Pb) to 1.4x10^{10} Ω.cm as shown in Figure 4. Complex impedance plots at temperatures exceeding 300 °C also showed the presence of a secondary semi-circle at low frequency range which is generally associated with grain boundary contribution (Fig. 5).

---

[1] Last column shows oxygen measured by the Oxygen Determinator. Three repeats were done on each powder sample. Due to the high oxygen content the sample size taken was around 5mg. The accuracy was estimated to be ± 0.25wt%.

Table II: Grain size and electrical properties of BiScO$_3$-PbTiO$_3$ ceramics with different excess contents.[2]

Composition	Grain size (μm)	ρ_{grain} (Ω.cm) at 55 °C	K$_{grain}$ at 55 °C	Relaxation frequency (Hz) at 325 °C	E$_{ac}$ (eV) from ρ	E$_{ac}$ (eV) from τ
No excess	24.8	4.1×10^{10}	1085	800	0.36	0.36
2% Pb	5.6	2.4×10^{10}	805	3000	0.35	0.32
5% Pb	1.3	1.4×10^{10}	727	5000	0.35	0.33
2% Bi	18.6	4.9×10^{10}	1104	400	0.40	0.40
5% Bi	3.35	19.6×10^{10}	1402	40	0.20 0.59	0.57

This inference was in agreement with the microstructural observations. The SEM micrographs in Figure 6 show that average grain size decreased from 24.8 μm for nominal composition to 5.6 and 1.3 μm for compositions containing 2% and 5% Pb, respectively (Table II). The decreased grain size with increasing PbO content is caused by formation of a PbO-rich liquid phase (T$_m$ $\approx$ 886 °C), which promotes formation of small prismatic grains [Fig. 6(d)]. These prismatic grains consisted of well-developed facets that were indicative of growth rate anisotropy. The faceted structure is a result of the PbO-rich liquid phase that wetted all surfaces, inhibiting grain coarsening and size [initial particle size was 1.1μm (Fig. 7)].[23] Thus, the effect of excess Pb content on the grain boundaries was two fold: (1) the excess PbO increased the grain boundary density and modified the grain morphology and (2) the increased concentration of the grain boundary phase increased electrical conductivity. As the PbO content increases, the area of the grain boundary phase, that is short circuiting the ceramic, would increase
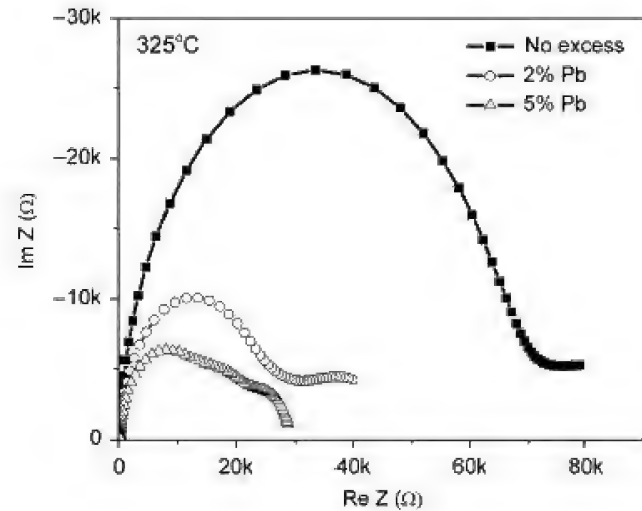
Fig. 5: Impedance results of BiScO$_3$–PbTiO$_3$ with 0%, 2%, and 5% excess Pb at 325°C measured from 1 Hz to 1 MHz.

resulting in further decrease in the resistance of the specimen. Inspection of relaxation frequencies (Table II) was in agreement with the explanation for the nature of PbO-rich grain boundaries and revealed that the conducting species needed a shorter period to reach to the electrodes as the excess Pb content increased. In addition to its effect on grain boundaries, excess Pb also changed the electrical properties of the grains. This suggested that some of the Pb contributed to the compensation of the Pb-deficiency. This can effectively result in a slight shift in composition towards higher PbTiO$_3$ content, which might be the reason for the shift in the phase transformation temperature with excess Pb content.
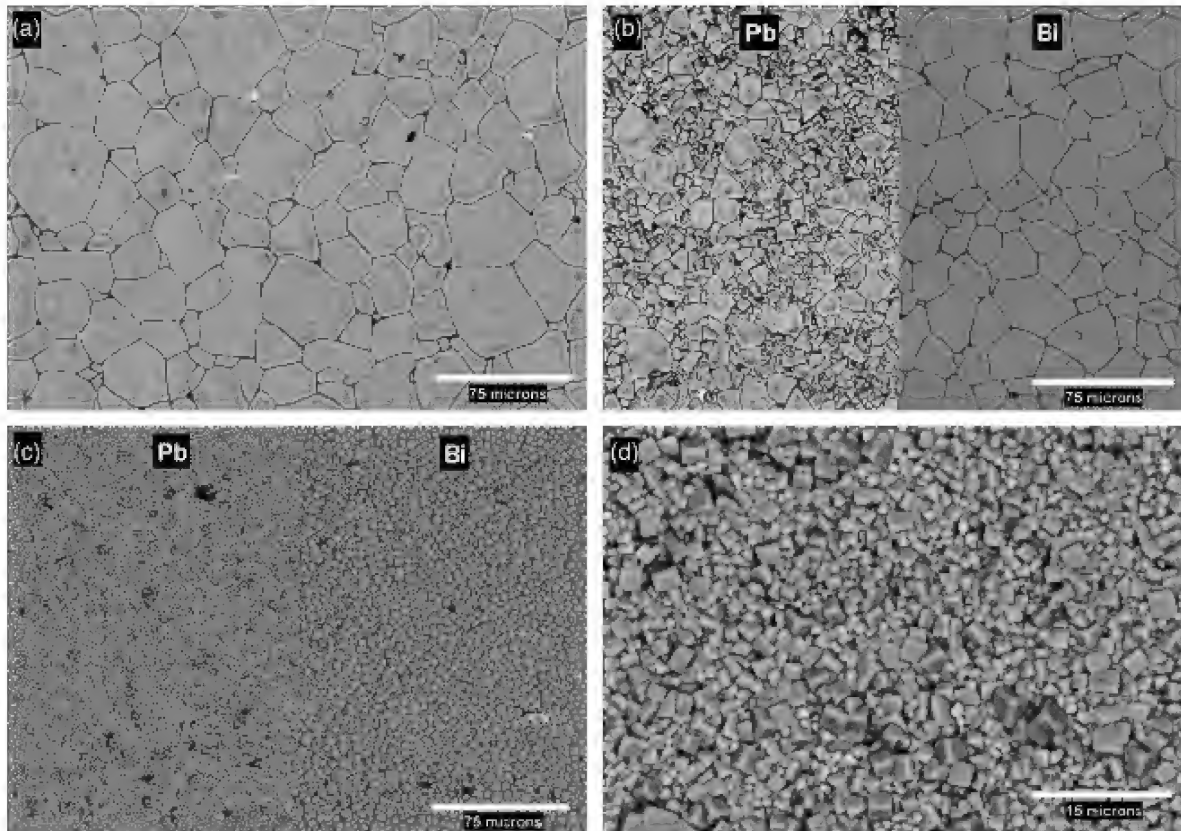
Fig. 6: Microstructure of sintered faces for BiScO$_3$–PbTiO$_3$ with (a) no excess, (b) 2% Pb and 2% Bi, (c) 5% Pb and 5% Bi, (d) 5% Pb at higher magnification.

The activation energy was calculated from the Arhenius plot of grain resistivity as a function of temperature using the relationship $\ln \sigma \propto E_{ac}/kT$, where σ, E_{ac}, k, and T are conductivity, activation energy, Boltzman constant and temperature, respectively (Fig. 8). The activation energy was ≈0.35 eV at 50 < T < 600 °C for all compositions, indicating that the conduction mechanism was the same. Activation energies calculated from the relaxation times (τ) summarized in Table II were 0.36 eV, 0.32 eV, and 0.33

eV for compositions with 0%, 2% and 5% Pb content. The comparison of activation energies calculated from conductivity measurements and relaxation times were in agreement. However, reported activation energy for ionic conduction in BS-PT system and similar perovskite systems was found to be ≥ 1eV and the activation energy for electronic conduction was around 0.1eV.[9,24,25] Our values are larger than the activation energies for electronic conduction calculated from single crystal BS-PT, but also was lower than that for ionic conduction.

Poling of BS-PT ceramics was conducted at 100 °C under 40 kV/cm for 10 mins. Composition with no excess Pb exhibited a relatively lossy hysteresis loop at the poling temperature, as shown in Figure 9(a). Strain under unipolar electric field of 50kV/cm was 0.17% [Fig. 9(b)]. The piezoelectric loops exhibited a large hysteresis and the calculated d_{33} was 354 pC/N. It was not possible to pole compositions with excess Pb due to the

Fig. 7: Particle size distribution of $BiScO_3-PbTiO_3$ powder before sintering.

increased electrical conductivity indicating the paramount importance of PbO content in this system.
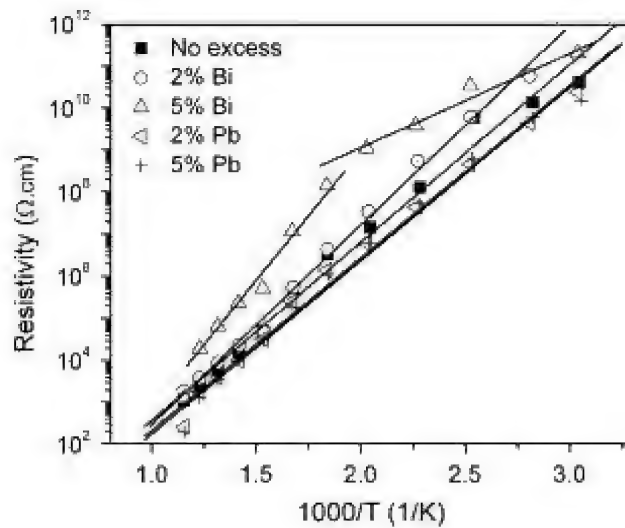
Fig. 8: Arrhenius type plots of grain resistivity calculated from equivalent circuit fitting as a function of temperature for $BiScO_3-PbTiO_3$ with 0%, 2%, and 5% excess Pb and Bi. Slope of the graph gives activation energy for the conducting species.

ii. **Excess Bi_2O_3**: Excess Bismuth addition did not have any effect on the Curie temperature but had significant effect on bulk resistivity, as shown in Figure 10. The samples containing 5% Bi had 19.6 $x10^{10}$ Ω.cm resistivity, which is 4.8 times larger than the nominal composition ($4.1x10^{10}$ Ω.cm).

The employment of excess Bi is expected to contribute two ways: (1) the substitutional Bi cations can take place for the cation losses occurring at the Bi and Pb sites during calcination and sintering, and (2) formation of a grain boundary phase. These two possibilities are not exclusive of each other. If excess Bi replaces the Bi lost during calcination, it would result in lower A-site vacany concentration compared to the nominal composition. Such replacement would have effects similar to

Fig. 9: (a) Bipolar field induced polarization for $BiScO_3$–$PbTiO_3$ with 0% excess, 5%Pb, 5% Bi,
(b) Unipolar field induced strain for $BiScO_3$–$PbTiO_3$ with 0% excess, 5%Bi.

acceptor doping. If the excess Bi replaces the Pb lost during processing, it would be a donor additive and enhance an A-site deficient system or decrease the hole conductivity for a p-type conductor.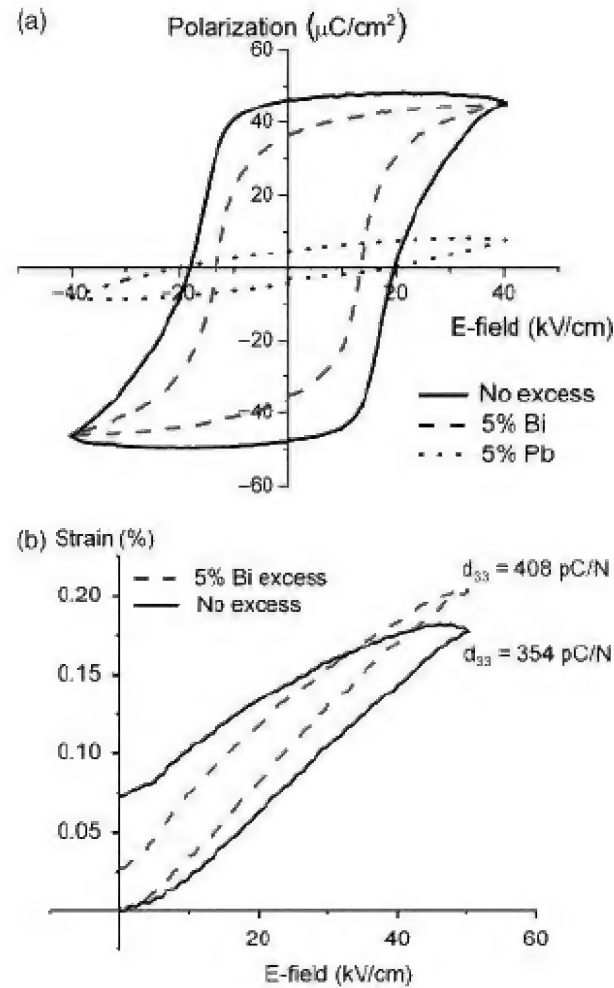 Donor doping in PZT results in increased resistivity and dielectric constant,[26] which is consistent with the observed properties of BS-PT system with excess Bi addition (Table II). It is highly likely that Bi would be replacing both Pb and Bi vacant sites. The concurrent increase in resistivity and dielectric constant with excess Bi addition supports the view that excess Bi is behaving like a "net" donor additive.

The average grain size was 18.6 and 3.35 μm for compositions with 2% and 5% Bi, respectively (Table II). The excess Bi_2O_3 is expected to form a liquid phase ($T_m \approx 817$ °C) during sintering. This liquid phase hinders grain growth (Fig. 6). The comparison of average grain sizes for the excess PbO and excess Bi_2O_3 compositions revealed that Bi_2O_3 was not as effective as PbO in limiting the grain growth. The grain morphology consisted of smaller size grains rounded around the triple points. Both the grain size and grain morphology indicated that the (i) liquid phase volume was lower for Bi addition than Pb addition of the same atomic percentage and (ii) Bi_2O_3(l) has a smaller wetting dihedral angle. The molar volume of Bi_2O_3 is 26.2 cm^3 (per one mole of Bi), which is slightly larger than the molar volume of PbO (23.4 cm^3) and thus it is unlikely that the observed microstructural differences are due to the differences in molar volume. These results suggest that the wetting characteristic of Bi-rich liquid phase was significantly
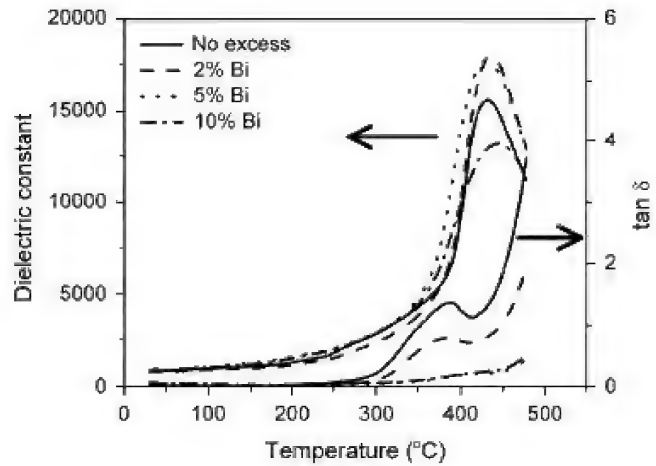

Fig. 10: Dielectric constant and loss tangent (at 10 kHz) as a function of temperature for compositions with 0%, 2%, 5%, and 10% excess Bi.
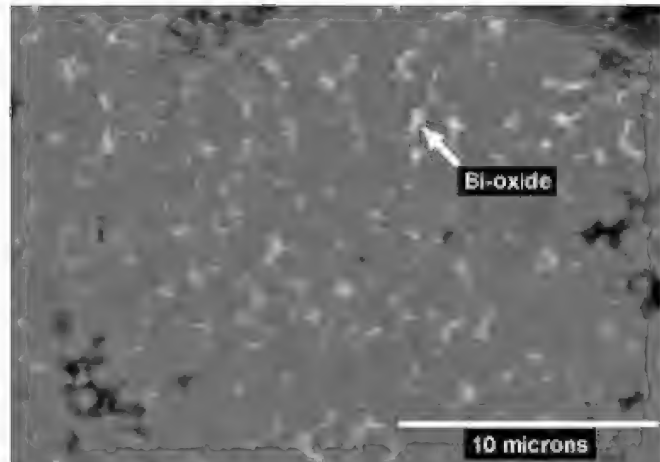

Fig. 11. Microstructure of sintered faces for $BiScO_3$–$PbTiO_3$ with 10% Bi (polished, unetched) showing pockets of Bi_2O_3 between the grains.

11

different than those of Pb-rich system and Bi-rich liquid phase does not wet the surface of the grains. This would suggest the formation of a non-continuous grain boundary phase of Bi_2O_3 concentrated at the triple points rounding the grains, consistent with microstructural observations. The XRD analysis of sintered specimens contained peaks for Bi_2O_3, in addition to the perovskite phase, indicating that the liquid phase crystallized upon cooling. This XRD observation is consistent with the formation of a second phase with larger volume at the triple points, rather than wetting the grain surfaces since the continuous thin films formed on the surfaces in general stay amorphous upon cooling.[23] SEM micrograph of a polished and unetched surface of specimen with 10%Bi excess shows these large pockets of Bi_2O_3 (Fig. 11).

The loss tangent decreased significantly with the addition of excess Bi. At temperatures exceeding 350 °C; tan δ at 10 kHz was 0.9, 0.6, 0.1 and 0.1 for Bi contents of 0%, 2%, 5% and 10%, respectively. Despite the decrease in tan δ for 2% excess Bi, the temperature dependence of tan δ was reminiscent of the base composition, as was the microstructure. The decrease in tan δ was more significant when 5% excess Bi was added and no runaway increase in conductivity was observed up to 475 °C. Addition of 10 % Bi did not increase the resistivity of the ceramics. The complex impedance plots at elevated temperatures (Fig. 12) exhibited only one semicircle indicating that there was only the grain contribution to resistivity despite a significant decrease in the grain size. The absence of grain boundary contribution was consistent with the formation of a non-continuous grain boundary phase. Therefore the increase in resistivity could be due to i) decreased grain size, and/or ii) "net" donor doping.

Relaxation frequency decreased with increasing excess Bi content at a given temperature, consistent with increased resistivity (Table II). The activation energies calculated from the Arhenius plot of resistivity (Fig. 8) revealed that the activation energies were in the same range (≈0.36-0.40 eV) for all compositions (for nominal, excess Pb and excess Bi) except for the specimens with 5% Bi. This composition
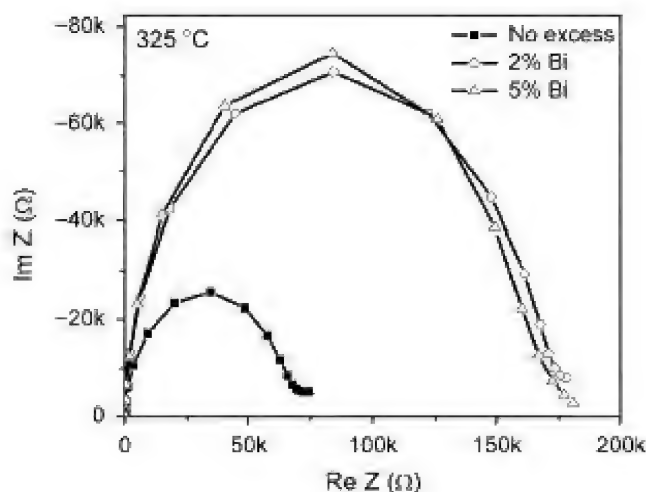

Fig. 12: Impedance results of $BiScO_3$–$PbTiO_3$ with 0%, 2%, and 5% excess Bi at 325°C measured from 1 Hz to 1 MHz.

12

exhibited a change in slope around 270 °C. The activation energies calculated from resistivity data were 0.2 eV for T < 270 °C and 0.59 eV for T> 270 °C. The temperature where the slope changed (270 °C) also corresponded to the temperature where the relaxation was first detected for this composition. The activation energy calculated from the relaxation times (τ) was similar in value (0.57 eV) for T > 270 °C (Table II). Despite the increase in the activation energy, these values were still lower than the activation energies calculated for ionic (oxygen) conduction (>1eV) in other ferroelectric perovskites.[24,25] A more in depth investigation to elucidate the conducting species and associated mechanisms is required.

The higher resistivity of the Bi added compositions made it possible to successfully pole these specimens (at 100 °C under 40 kV/cm for 10mins). Polarization measurements conducted under bipolar field after poling at 100 °C showed a narrow and saturated hysteresis loop [Fig. 9(a)]. The coercive field E_C and the remnant polarization P_R for composition with 5% excess Bi at 100 °C were 13.5 kV/cm and 38 $\mu C/cm^2$, respectively. Piezoelectric coefficient (d_{33}) is defined by the slope of the field induced strain graphs. Due to the non-linear nature of the piezoelectric behavior at high fields, d_{33} changes as a function of electric field. As an approximation, d_{33} is defined as the maximum strain to maximum field ratio. The improved poling conditions of composition with excess Bi led to enhancement of piezoelectric coefficient (d_{33} = 408 pC/N at 100°C whereas the base composition exhibited a d_{33} = 354 pC/N). Field induced strain was >0.2% under 50kV/cm and exhibited less hysteresis for compositions with 5% excess Bi [Fig. 9(b)].

iii. **High temperature properties:** BS-PT ceramics mixed with excess 2.5%Bi_2O_3 (5%Bi) was chosen as the most promising composition and the high temperature measurements were focused on this system. The high temperature electrical and electromechanical properties were measured under weak and high electrical fields for both solid state sintered and liquid phase sintered 37BS-63PT composition. Because the samples contained 0 and 5% Bi (2.5%Bi_2O_3), they will be referred to as B0 and B5, respectively.

a. *Weak electric field properties:*
Liquid phase sintering using excess Bi_2O_3 decreased the dielectric loss at elevated temperatures, as discussed in previous section (Figure 13). The temperature dependent dielectric constant exhibits similar behavior for both B0 and B5. Table III shows the values for dielectric constants and dielectric losses for both B0 and B5 at elevated temperatures. Dielectric constant (1kHz) at 100 °C was ≈ 1030 for B0 and ≈ 1175 for B5.

Table III: Dielectric properties of solid state sintered (B0) and liquid phase sintered (B5) specimens at elevated temperatures:

Temperature	B0			B5		
	K'	tan δ	K''	K'	tan δ	K''
100 °C	1031	0.022	23	1175	0.037	43
200 °C	1411	0.183	258	1730	0.06	104
300 °C	3669	1.302	4777	3279	0.093	305

The B5 sample had higher dielectric loss at low temperatures (<205 °C) but the B5 composition exhibited a lower dependence on temperature. Therefore at higher temperatures (>205 °C) B5 exhibited lower dielectric loss (Fig. 13 and Table III). Liquid phase sintering reduces the dielectric loss, causing a reduction in AC-conductivity (σ_{ac}) at elevated temperatures. The AC-conductivity (σ_{ac}) is dependent on the dielectric loss ($\varepsilon_r^{''}$) as represented by the equation: $\sigma_{ac} = \omega \varepsilon_0 \varepsilon_r^{''}$ where ω and ε_0 are the angular frequency and the permittivity of free space, respectively.[27] Retention of AC-resistivity at elevated temperatures is highly desirable for engineering applications of actuators.

Microstructural contribution to electrical properties were studied by electrical impedance spectroscopy to differentiate the grain and grain boundary contributions.[28] Figure 14(a) shows the equivalent circuit to model the electrode, grain and grain boundary contributions to impedance. The grain boundary contribution could not be deconvoluted from the spectrum for either composition. The complex impedance plots are single semicircles with a single relaxation frequency up to 600 °C (Figure 12). Grain resistance calculated from equivalent circuit analysis for specimens of same geometry showed an increase from 4.1×10^{10} Ω for B0 to 19.6×10^{10} Ω for B5 at around 50°C. The
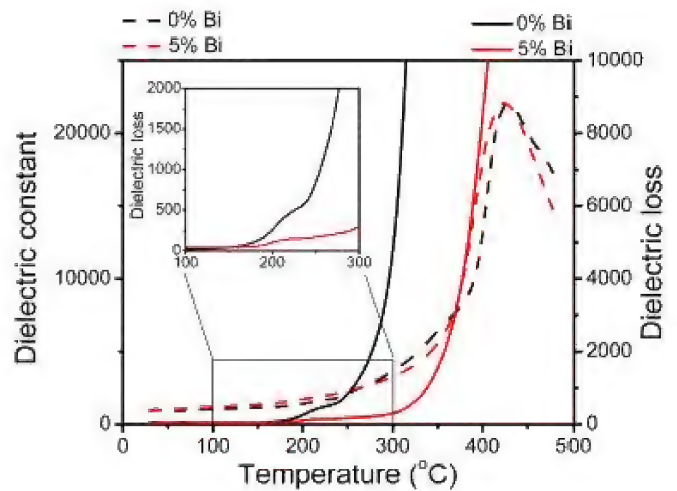

Fig. 13: Dielectric constant and dielectric loss as a function of temperature for B0 and B5 at 1kHz.

increased resistance can be a sign of increased number of interfaces in B5 which had an average grain size of 3.35µm, significantly lower than that of B0 (24.8 µm).

The dielectric constant calculated from the impedance data at 100 °C was 1550 and 1700 for B0 and B5, respectively. The phase angle ranges from -85° and -90° for the frequency range 1Hz-1MHz for B5; indicating that the impedance is dominated by capacitive reactance and the voltage lags the current by almost 90° [Fig. 14(b)].[28] For B0 composition, the phase angle ranges from 85° and 90° for frequencies >500Hz [Figure 14(b)]; the results suggest the impedance is dominated by capacitive reactance. At lower frequencies (<500Hz) the phase angle decreases with decreasing frequency down to -49° at 1Hz; the impedance has both capacitive and resistive components.

Solid state sintered samples (B0) were more electrically conductive than liquid phase sintered samples (B5). The diffused resonance peaks lead to uncertainity in calculating the electromechanical coefficients from the resonance-antiresonance peaks. In contrast, liquid phase sintered ceramics (B5) were more resistive and exhibited sharp resonance peaks. Using disc shaped specimens with an aspect ratio of 10:1, transverse piezoelectric coefficient (d_{31}), and planar electromechanical coefficient (kp) were calculated as specified in IEEE standards.[29]
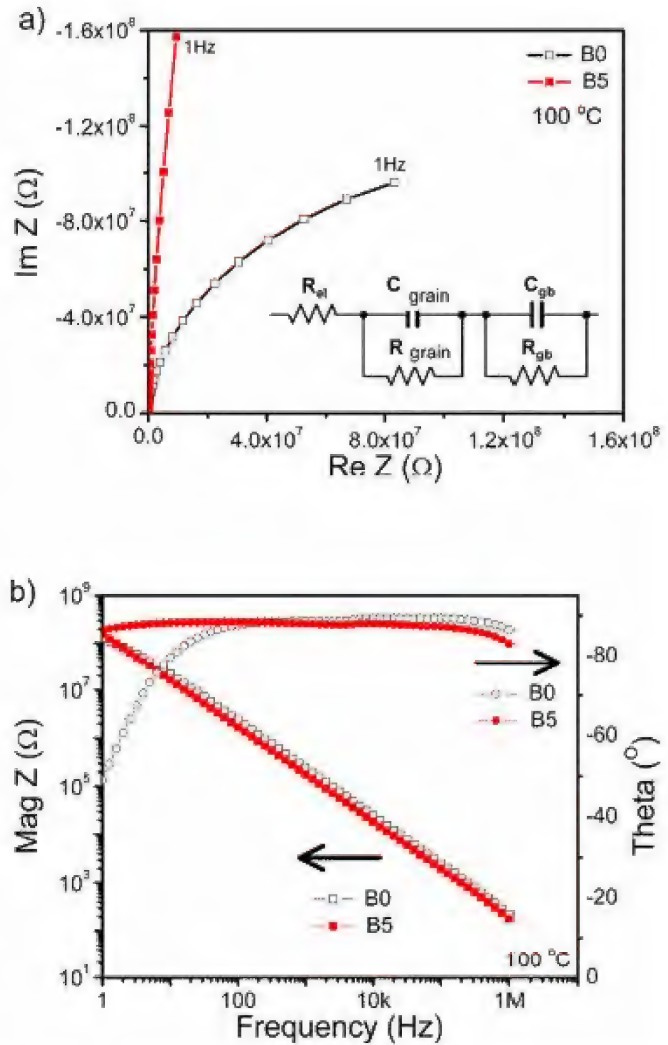

Fig. 14: (a) Complex plot of impedance from 1Hz to 1MHz at 100 °C for B0 and B5, (b) Magnitude of impedance and phase angle (theta) as a function of frequency at 100 °C for B0 and B5.

Figure 15 shows planar electromechanical coupling coefficient (k_p), transverse piezoelectric coefficient (d_{31}) and dielectric constant (K_{33}) as a function of temperature. The transverse piezoelectric coefficient (d_{31}) increased with temperature from -85 pC/N to -211 pC/N ; the maximum d_{31} occurred at 352 °C. The maximum temperature for dielectric constant (430 °C) and d_{31} differ by 78°C. The structure gets softer as the phase transformation temperature is approached, causing an increase in dielectric constant up to the Curie Temperature (T_c= 430 °C). However,
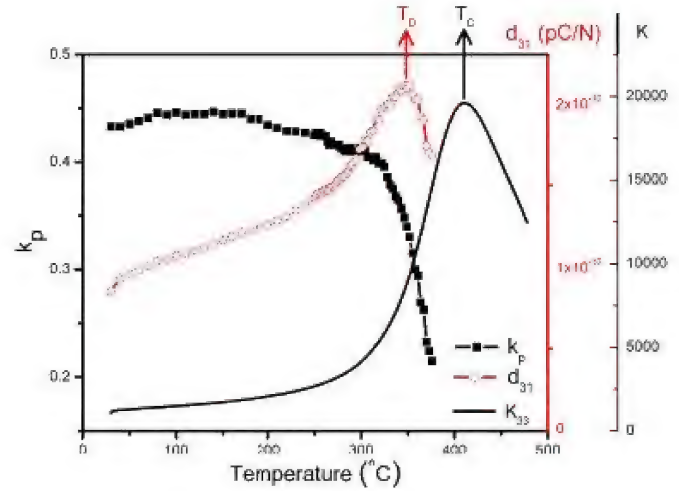

Fig. 15: Planar electromechanical coupling coefficient (k_P), transverse piezoelectric coefficient (d_{31}) and dielectric constant (K) of B5 as a function of temperature. Depoling temperature (Tʙ) and the Curie Temperature (Tᴄ) aremarked on the graph.

elevated temperatures below T_c are sufficient to assist dipole rotation and depoling. Unpoled materials do not exhibit piezoelectricity, thus the piezoelectric coefficient reduces as the material starts to depole. Thus for B5, depoling is observed at temperatures lower than the Curie temperature. A rapid depoling rate would be detectable by capacitance measurements. The absence of such peaks suggests a slow depoling rate. In fact, it was possible to detect the fundamental resonance peaks up to 433 °C. Further investigations are required to determine the depoling rate and will not be further discussed.

Calculated planar electromechanical coupling coefficient (k_p), as specified in IEEE standards, was 0.43 at room temperature and maintained a value >0.4 up to 320 °C. Above 300 °C, the coupling coefficient decreased to 0.15 at 400 °C (Fig. 15). This gradual decrease in k_p also suggests depoling is rather a slow process in the BS-PT system. The maximum d_{31} (352°C) lies in the depoling temperature range (300-430°C). The corresponding k_p for the maximum d_{31} was 0.35.

b. High electric field properties:

Bipolar field induced polarization behavior for B0 and B5 is presented in Figure 9(a). B0 samples exhibit a "lossy" hysteresis loop, indicating that there is leakage parallel to the insulator at high electric fields. The highly resistive B5 exhibits a saturated hysteresis loop. The remanent polarization (P_r) and coercive field (E_c) of B5 were 38 μC/cm^2 and 14 kV/cm at 100 °C. However, the E_c and P_r for B0 could not be measured directly from the bipolar hysteresis loops. Both coefficients are dependent on the applied

electric field and frequency; E_c and P_r determination is impractical for significant current leakage [Fig. 16(a)]. Such dependence on the applied field did not exist for liquid phase sintered samples B5 [Fig. 16(b)]. Unipolar polarization loops are presented to show the frequency dependence of ferroelectric properties. For B0, measurements at lower frequencies resulted in widening of unipolar polarization loops, due to the increased time allowed for space charge (free charge) to travel [Fig. 17(a)]. The dependence on measurement frequency for B5 was significantly less as a result of decrease in current leakage due to high resistivity [Fig. 17(b)].

In figure 17(a), a unipolar ferroelectric loop for B5 measured at 1Hz is shown with the loops for B0 for comparison. A significant difference was observed between the slopes for B0 and B5, indicating a difference in capacitive behavior, and resistive behavior as discussed earlier. The slope of the field induced polarization (P vs. E) loops is related to dielectric constant, and thus the capacitance. The
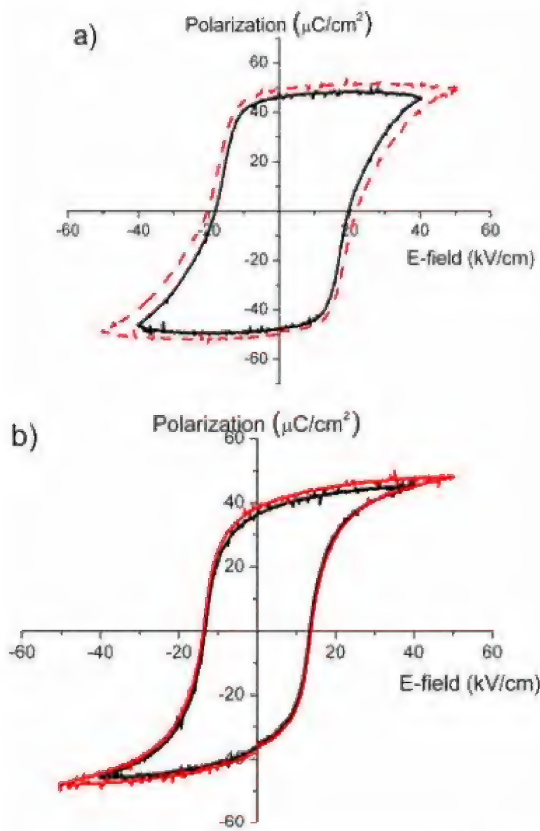

Fig 16: Effect of the magnitude of the applied field on the ferroelectric properties for (a) B0 and (b) B5.
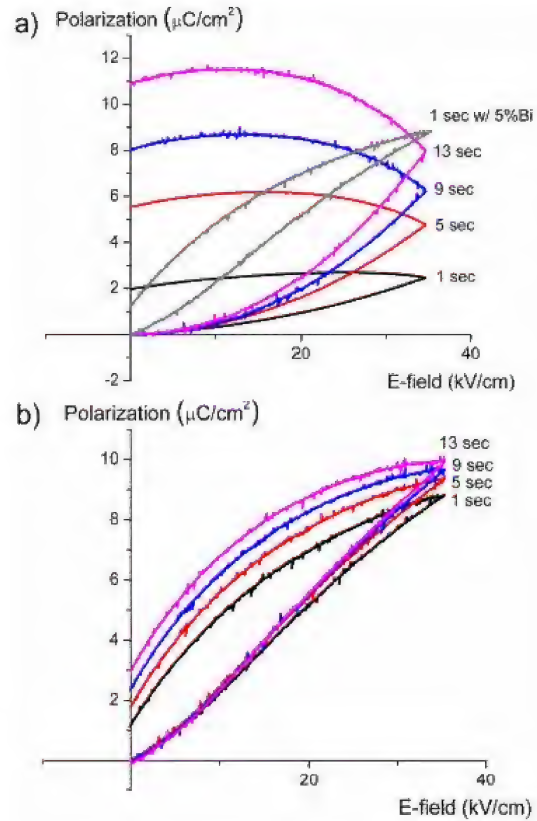
Fig 17: Effect of the frequency of the applied field on the ferroelectric properties for (a) B0 and (b) B5. B5 measured at 1Hz is projected in the part (a) for comparison.

relationship between P and E is defined by the equation $P=\varepsilon_0(K-1)E$; where P is the polarization, ε_0 is the permittivity of free space, K is the dielectric constant and E is the applied electric field.[27] Neither B0 nor B5 are linear capacitors. The capacitance is dependent on the applied electric field; high electric fields cause domain re-orientation and saturation of charge separation.

Below 5kV/cm, the P vs. E loops could be fitted with a linear equation for both B0 and B5. Dielectric constant (K) was calculated from the slope; 320 for B0 and 2100 for B5. The dielectric constant calculated from P vs E loops (2100) was higher than the dielectric constant (1175) obtained by weak field impedance measurements for B5. The difference can be due to two effects; i) measurement frequency (1Hz vs. 1kHz) and ii) applied electric field (5×10^{-3} kV/cm vs. 50kV/cm). As discussed earlier, impedance of B5 is dominantly capacitive reactance. Thus, the dielectric constant increases with decreasing frequency. However, frequency dependency alone is not likely to explain the large difference between the values. For the assumption of pure capacitive reactance, the frequency change (from 1kHz to 1Hz) would only result in an increase from 1175 to 1340, a 14% increase(as calculated from $\left|Z\right| = Z^{''} = \dfrac{1}{\omega C}$ using the weak field measurements, where Z, ω and C are impedance, angular frequency and capacitance, respectively). Further contributions can be due to the larger electrical field where the higher order terms cause non-linear behavior. Even though the high field dielectric constants were calculated from the slope of the linear part of the P vs E loops, the behavior can be significantly different than the weak field measurements and could not be extrapolated to weak field region. While the field for the weak field measurement was 5×10^{-3} kV/cm, the resolution of data in high field measurements was 150×10^{-3} kV/cm. Therefore the field for first data point of P vs E loops was thirty times higher than the weak field of impedance measurements. For B0 the dependence of the dielectric constant on electric field and measurement frequency is complex
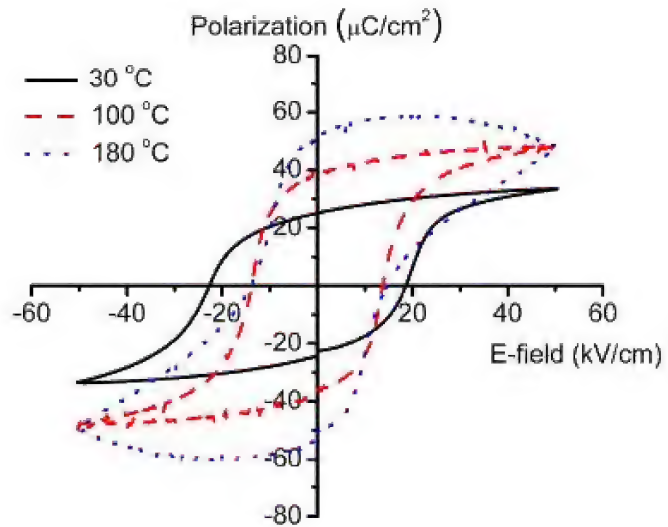

Fig 18: Effect of temperature on the ferroelectric properties of B5.

due to presence of free charges and associated high conductivity. Assumptions (i.e., pure capacitive reactance) made for the discussion of B5 composition is not valid for B0.

Figure 18 shows the bipolar field induced polarization for liquid phase sintered B5 as a function of temperature. The E_c and P_r at room temperature were $\approx$ 20 kV/cm and 25 $\mu C/cm^2$. The loops showed a shift of approximately 2kV/cm opposite to the poling direction. At 100 $^\circ$C, as expected for thermally assisted polarization rotation, P_r increased (38 $\mu C/cm^2$) and E_c decreased (14 kV/cm). At 180 $^\circ$C, specimens were more "lossy" at high fields and P_r cannot be determined. The coercive field was same at 100 $^\circ$C and 180 $^\circ$C ($\approx$14kV/cm).

High field induced strain measurements for the liquid phase sintered B5 are presented in Figure 19. Liquid phase sintering increased the resistivity and improved the poling characteristics which resulted in a 15% increase in d_{33}. The strain achieved at 100 $^\circ$C for B5 was approximately twice the value obtained at 20 $^\circ$C ($\approx$0.1% and 0.2% at 20 $^\circ$C and 100 $^\circ$C, respectively). Piezoelectric coefficient (d_{33}) is defined by the slope of the field induced strain graphs. Due to the non-linear nature of the piezoelectric behavior at high fields, d_{33} changes as a function of electric field. As an engineering approximation, we can define d_{33} as the maximum strain to maximum field ratio. For such an approximation, $d_{33} \approx$ 200 pC/N and $\approx$ 400
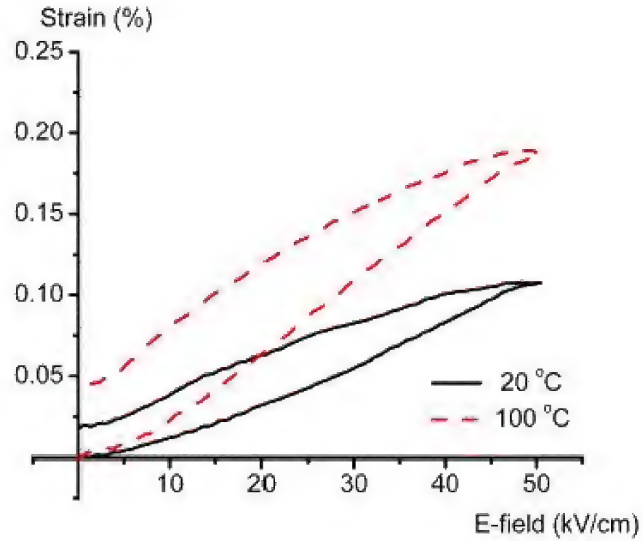

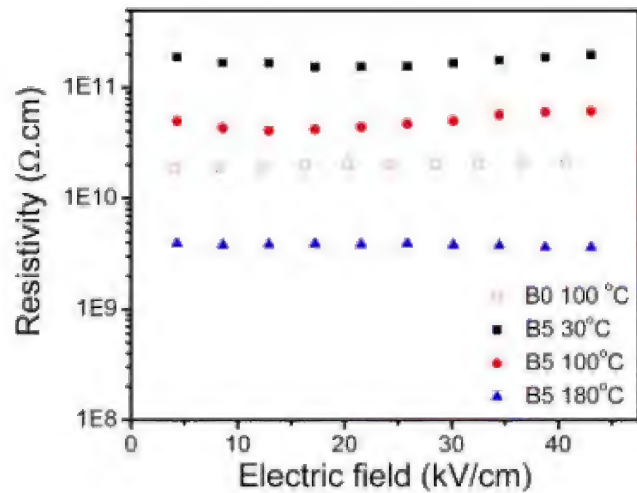**Fig. 19:** Effect of temperature on the piezoelectric properties of B5.

Fig. 20: High field DC-resistivity of B0 and B5 as a function of temperature and applied field.

pC/N at 20 ^{o}C and 100 ^{o}C, respectively. As the temperature increases the structure softens and allows larger displacement under electric field. Thus, the piezoelectric coefficient increases with increasing temperature up to the temperature where depoling starts. Measurements of direct piezoelectric coefficient at room temperature by a Berlicourt type d$_{33}$-meter showed d$_{33}$ ≈ 208 pC/N.

High field DC-resistivity of B5 is shown in Figure 20. DC-resistivity at room temperature is >10^{11} Ω.cm up to 45 kV/cm and decreases down to ≈ 5x10^{10} Ω.cm at 100 ^{o}C and ≈ 3x10^9 Ω.cm at 180 ^{o}C. B0 exhibited a DC-resisitivity of ≈ 1x10^{10} Ω.cm at 100 ^{o}C, one fifth of the liquid phase sintered B5 with excess Bi$_2$O$_3$ (Fig. 20) confirming the improved resistivity of liquid phase sintered BS-PT ceramics.

2.   Compositional Engineering:

The state of the art materials for high temperature applications are Pb(Zr,Ti)O3 (PZT) – based ceramics. PZT ceramics have been investigated for several decades and as a result of different doping strategies they have been modified to satisfy a wide range of specifications (i.e., high power, high temperature, large response etc.). Soft PZTs were designed to create large response (piezoelectric coefficient d$_{33}$ = 750 pC/N for Navy Type IV / PZT 5H) but were limited by low Curie temperatures (T$_c$ = 195 ^{o}C) and increased dielectric losses (loss tangent tan δ = 0.05). Hard PZTs were used for high power or high temperature applications and were designed to have higher Curie temperatures (T$_c$ = 370 ^{o}C for Navy Type II / PZT 5A) and low dielectric losses (tan δ = 0.005) but the piezoelectric displacement attainable was also limited (d$_{33}$= 375 pC/N). There hasn't been any significant development in this mature industry over a decade.

Similar to the history of piezoceramics development based on PZT, different doping strategies were taken to improve the BS-PT piezoceramics as a part of **Task I**. The high temperature dielectric, ferroelectric and electromechanical properties are also reported for the doped BS-PT ceramics as a part of **Task III**. Isovalent (In, Yb), aliovalent (Sr, Zr) and multivalent (Mn) cations were chosen as dopants. BiInO$_3$ (BI) and BiYbO$_3$ (BY) are believed to have the highest T$_c$ at their MPB compositions in solid solution with PT. However, neither of the two can be processed as a pure perovskite. Only BI and BY binaries that can be processed contain a large level of PT resulting in very conductive ceramics. The objective of In and Yb doping to the place of Sc was to increase the Tc while keeping the structure still a perovskite. Even though single phase materials were processed, the resulting ac-conductivity was much higher. By exploring ternary MPBs based on BiInO$_3$-BiScO$_3$-PbTiO$_3$, it was possible to increase the Curie temperature up to 500°C. However, the leakage at high fields was too high even to pole these

compositions. Liquid phase sintering to increase the resistivity did not have the similar effect observed in binary system. Therefore further work on this type of dopant was discontinued.

Mn doping was successful in increasing the piezoelectric coefficient and was a promising dopant to increase the electromechanical activity of the ceramics. However, Mn doping significantly decreased the T_c and the polarizability of the ceramic. In addition, the poled domain structure became less stable, resulting in a larger difference between saturated polarization and remanant polarization.

Donor doping using Zr improved the BS-PT based high temperature piezoelectrics significantly. Therefore most of the research focused on this type of dopant. Following is the summary of the effects of donor (Zr) doping. Discussion will concentrate on three groups of results: (i) Weight loss studies, (ii) Structural analysis, and (iii) electrical and electromechanical properties.

i. **Weight loss studies:** Doped composition was formulated with 2% $Zr_{Sc}^{\cdot}$. The weight loss for the undoped composition during sintering was <2 wt.%, which is similar in value to published data.[3] TGA analysis showed a weight loss of 0.17% with onset at 1030 ^{o}C upon heating (Fig. 21). Weight loss graphed in Figure 21 is normalized at 450°C to compensate for different levels of weight loss at lower temperatures associated with the loss of physically bonded water. The weight loss at high temperatures is generally attributed to high vapor pressure of Pb and Bi at sintering temperatures. ICP analysis of the volatilized species collected by condensation on a water cooled Cu-plate indicated that Pb loss was much higher than Bi loss with a distribution of 91%Pb to 9%Bi (Table IV).

ICP analysis was conducted on several batches of the same composition $0.37BiScO_3-0.63PbTiO_3$. The Bi/(Bi+Sc) ratio varied between 0.36-0.37 and Sc/(Sc+Ti) ratio was between 0.36-0.38 (Table IV). The results indicated possible heterogeneities from batch to batch and within the same batch. In either case there has not been a major shift in the composition away from the batched formula.

Doped compositions showed similar compositional ratios of 0.36 and 0.37-0.38 as calculated from Bi/(Bi+Sc) and Sc/(Sc+Ti), respectively. Zr-content was
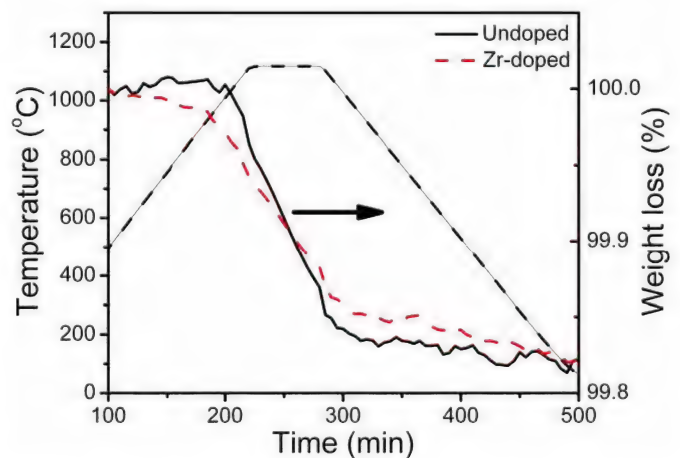

Fig. 21: Thermo-gravimetric analysis of undoped and Zr-doped BiScO$_3$-PbTiO$_3$ piezoceramics during sintering.

0.14 mol% which was practically equal to the theoretical amount 0.148 mol%. TGA analysis of doped compositions revealed weight loss of 0.18% during sintering, similar to the undoped composition. Weight loss of the doped material was more gradual than that observed for the undoped composition (Figure 21). The volatilized components were 90%Pb and 10%Bi (Table IV). However, the weight measurements of actual Zr-doped BS-PT samples before and after sintering showed a weight gain of 0.15-0.3% (Table IV). The difference between the TGA measurements and the actual weight change can be related to sintering conditions. No sacrificial powder was used during the TGA measurements. Therefore the weight gain can be associated with high Pb and Bi partial pressure during the actual sintering.

Weight gain has been observed in donor doped PZT systems with Pb content lower than the stoichiometric amount. The ceramics can pick up Pb from the surrounding atmosphere. For the donor doped BS-PT ($Zr_{Sc}^{\cdot}$), charge balance can be achieved by cation (Pb, Bi) loss, pick-up of oxygen, change of oxidation state of Ti or $Pb_{Bi}^{/}$ replacement. Weight gain during sintering indicates that the charge balance through loss of cations is not the dominant mechanism. If the specimens were picking up oxygen, both TGA measurements and the actual sintering measurements would show a weight gain since in both cases oxygen gas was flowing. The contradictory results might indicate a complex charge balance system of Pb pick up on Bi-sites. XRD analysis showed Bi-sites to be available in the perovskite lattice due to formation of a Bi-containing second phase and this will be discussed further in section (ii). Our results show that measurements of charge balance mechanisms are complicated through relative ratios of Pb- and Bi-loss, and differences between measurement conditions and actual processing conditions such as the use of sacrificial powder and even the composition of the sacrificial powder.

Table IV: Compositional and microstructural analysis of doped and undoped BiScO₃-PbTiO₃

	Bi/(Bi+Pb)	Sc/(Sc+Ti)	Weight change (%) During sintering	Weight change (%) TG	Volatilized species	Grain size (μm)
Undoped	≈36	≈38	-<2	-0.17	91Pb-9Bi	>20 (bimodal)
Doped	≈ 36	≈ 37.5	+0.15-0.3	-0.18	90Pb-10Bi	≈2

ii. **Structural analysis:** Lattice parameters are given in Table II for both undoped and doped compositions as measured by X-ray Diffraction and calculated using TOPAS v.3 s/w (Bruker AXS). LeBail method was used with no structural model input. Only space group and estimated starting lattice parameters were introduced. Excellent fits were observed for a mixture of rhombohedral and tetragonal lattice (Fig. 22). In addition, a minor secondary phase of $TiBi_{12}O_{20}$ was detected [Fig.22 (inset)] indicating that the perovskite phase was Bi deficient. The unit cell volume calculated for both rhombohedral and tetragonal phases were larger for the doped composition. A-site or oxygen vacancy formation in general results in a decrease in lattice parameters. Donor doping is expected to increase the A-site vacancies. However, as discussed in section (i) and as observed in the lattice calculations, it likely that a different charge balance mechanism is occurring. If Pb was picked up from the atmosphere to replace the Bi-vacancies in the perovskite phase, it would be expected to have an increase in weight during sintering and expansion of lattice parameters in comparison to the undoped composition. Both of these conditions were observed in the donor doped BS-PT ceramics.

The estimated weight fractions of rhombohedral and tetragonal phases are also given in Table V for both compositions. These estimates are based on the ratio of the intensities of the strongest peaks of the phase profiles generated for lattice parameter calculations. The assumptions made for these estimates were: (i) Contribution of $TiBi_{12}O_{20}$ phase is insignificant, (ii) relative intensity ratio (RIR) factors for
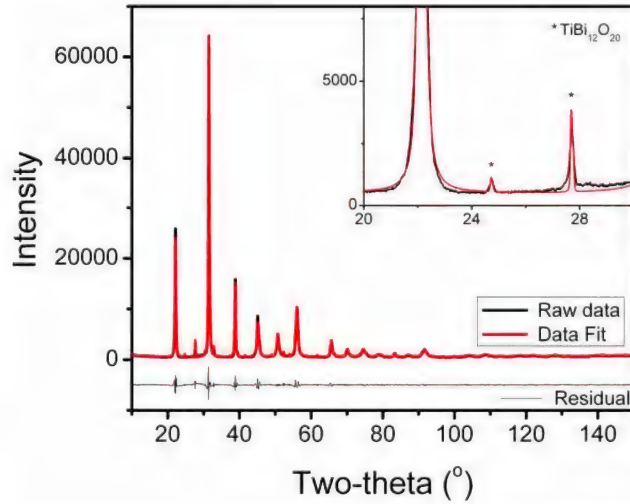
Fig. 22: X-ray Diffraction of doped composition. Inset highlights the secondary phase.

Table V: Lattice calculations of doped and undoped $BiScO_3$-$PbTiO_3$[1]

| | tetragonal perovskite | | | rhombohedral perovskite | | $Ti Bi_{12} O_{20}$ |
	a (Å)	c (Å)	c/a	a (Å)	α (°)	a (Å)
Undoped	3.988	4.055	1.017	4.019	89.80	10.191
Doped	3.997	4.052	1.014	4.027	90.16	10.198

[1] Error bars are estimated to be ~ 0.003 Å based on variations in repeated fitting runs.

both phases are equal, and (iii) profile shape of each phase is the same. Zr-doped composition has a greater amount of rhombohedral phase (71R-29T) in comparison with undoped composition (53R-47T). In addition, the tetragonality (c/a) of the T-phase was lower for the doped specimen (Table V). Despite the lower accuracy of such estimates, the large shift in the ratio observed indicated that the undoped compositions were closer to the MPB.

SEM analysis showed that the grain size for the Zr-doped BS-PT was around 2µm, which is almost an order of magnitude smaller than undoped BS-PT. Such decrease in grain size was shown to increase the resistivity through liquid phase sintering when the grain boundary phase is not continuous. Therefore the effects of dopants in the BS-PT can be two-fold, direct contribution to the defect chemistry and indirect effect on the microstructure.

iii. Electrical and electromechanical properties:

I. Weak electric field properties:

Figure 3 shows dielectric constant and tan δ as a function of temperature for both undoped and doped compositions. Addition of 2% Zr decreases the T_c by 20° down to 404°C as exhibited by the peak of dielectric constant. Room temperature data is given for both doped and undoped compositions in Table VI. Doping did not have any significant effect on the room temperature loss tangent, however it increased the dielectric constant for all temperatures up to the Curie temperature. At room temperature, the dielectric constant increased from 920 to 1295 with doping. When normalized for the change in T_c (Fig. 23 inset), the dielectric constant was still higher for the doped composition (1020 and 1295 at room temperature for undoped and doped compositions, respectively). Such an increase is consistent with the donor doping effects in PZT ceramics.

Doped composition had higher depoling temperature (378°C) than the undoped composition (352°C) despite a decrease in Curie Temperature (Fig. 24). Depoling temperature was defined as the peak of transverse piezoelectric
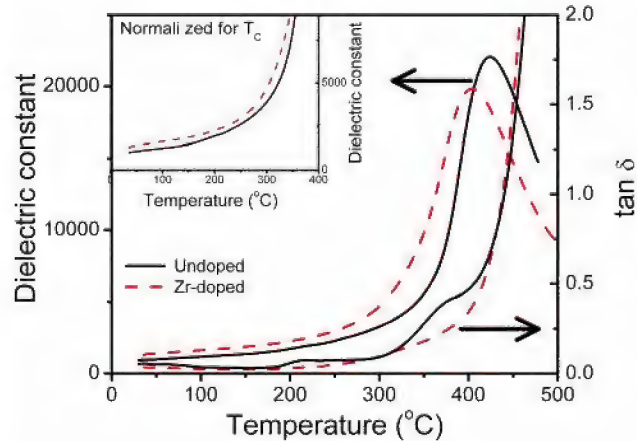

Fig. 23: Dielectric constant and tan δ at 1kHz as a function of temperature for both undoped and doped compositions. Inset shows the dielectric constant data normalized for the difference in Curie temperature.

24

coefficient (d_{31}). Using disc shaped specimens with an aspect ratio of 10:1, transverse piezoelectric coefficient (d_{31}), and planar electromechanical coefficient (k_p) were calculated as specified in IEEE standards.[11]

The transverse piezoelectric coefficient (d_{31}) and the planar coupling coefficients were -85pC/N and 0.43 for undoped and -69pC/N and 0.37 for the doped specimens. The decrease in electromechanical coupling coefficients is inconsistent with the effects of donor

Fig. 24: Electromechanical properties of undoped and Zr doped $BiScO_3$-$PbTiO_3$ piezoceramics as a function of temperature.

doping in PZT ceramics. The d_{31} increased with temperature maximizing at -211 pC/N for undoped and -200pC/N for doped specimens. As mentioned above the maximum d_{31} was at a temperature 26°C higher for the doped specimen. At elevated temperatures below T_c, the thermal energy is sufficient to assist dipole rotation and depoling. Unpoled materials do not exhibit a net piezoelectric effect, thus the piezoelectric coefficient reduces as the material starts to depole.

Calculated planar electromechanical coupling coefficient (k_p) for undoped specimen was 0.43 at room temperature and maintained a value >0.4 up to 320 °C. Above 320 °C, the coupling coefficient started to decrease significantly. The corresponding k_p for the maximum d_{31} was 0.35. The k_p for the doped specimen did not show a significant dependence on temperature up to 370 oC above which a sudden decrease was observed. The corresponding k_p for the maximum d_{31} was 0.28.

II.   *High electric field properties:*

Figure 25 shows the bipolar ferroelectric and piezoelectric behavior for both undoped and doped specimens at room temperature and at 100°C. The coercive field (E_c) was similar for both compositions at room temperature (19.25kV/cm and 20.33kV/cm) inconsistent with the effects of donor doping in PZT ceramics (Table VII). In general the effect of donor dopants in PZT is explained "on the basis of vacancies facilitating domain boundary motion" and donor doping decreases E_c in PZT ceramics. However as discussed in section (i), the charge balance system for the donor doped BS-PT system is more complicated than just A-site cation loss. At higher temperatures thermal energy assists polarization rotation, thus the coercive field decreases. At 100°C E_c was 13.95kV/cm and 14.25kV/cm for undoped
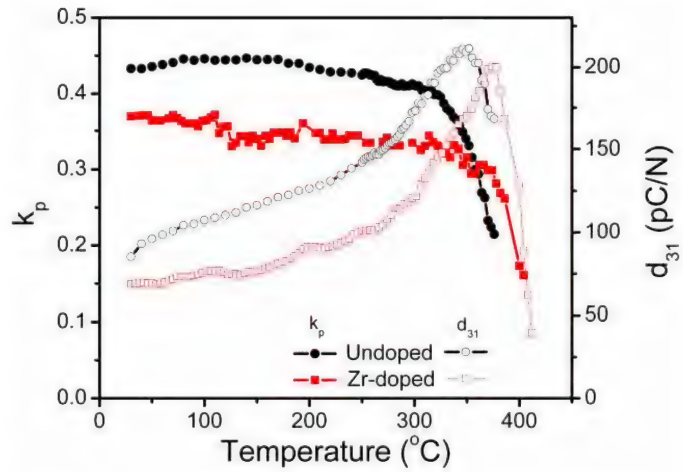
and doped specimens, respectively. The E_c calculated from piezoelectric loops were slightly lower but the trend as a function of temperature was similar (Table VII).

Aforementioned E_c values are the average of $-E_c$ and $+E_c$. Table VII also shows the deviation from the average. At room temperature loops for both undoped and doped compositions were asymmetric indicating domain pinning (Fig. 25). This effect was less observable for the doped specimen. The effects of doping on domain rotation are discussed later in this section in the light of all the measured properties. At high temperatures both compositions showed symmetric bipolar loops due to thermally assisted domain rotations.

Table VI: Dielectric properties of doped and undoped $BiScO_3$-$PbTiO_3$.

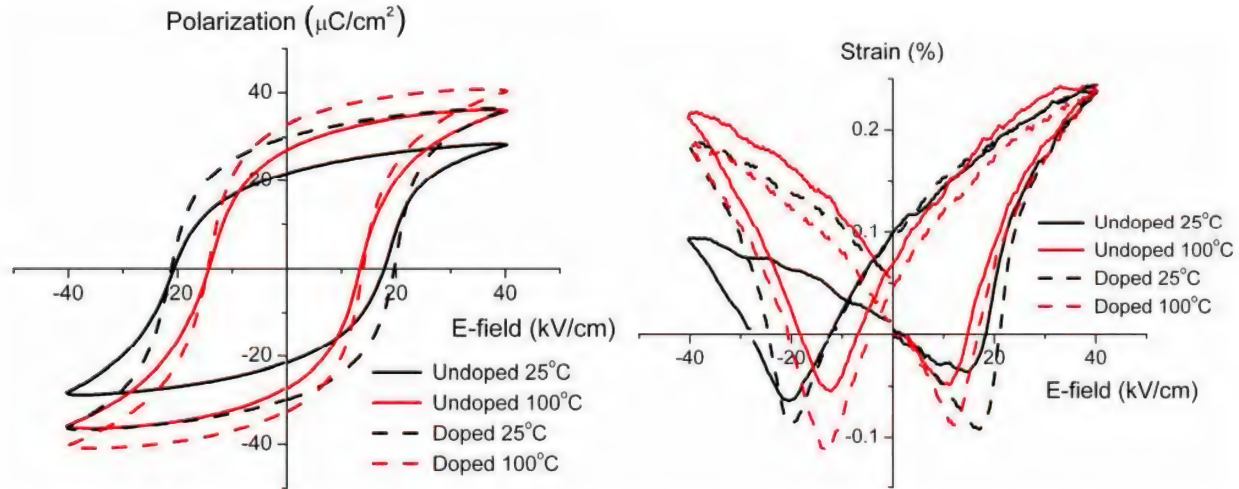|		Agilent 4294A				aixACCT		
	T_c ($^{\circ}$C)	K at 25°C	Norm. K at 25°C	tan δ at 25°C	K at 100°C	K at 25°C, 0kV/cm	K at 100°C, 0kV/cm	K at 25°C, 40kV/cm	K at 100°C, 40kV/cm
Undoped	424	920	1020	0.052	1175	920	1320	700	835
Doped	404	1290	1290	0.036	1615	1100	1405	730	810

Fig. 25: Bipolar **(a)** polarization and **(b)** strain measurements as a function of electric field at room temperature and at 100 $^{\circ}$C for both undoped and doped compositions.

Table VII: Ferroelectric and piezoelectric properties of doped and undoped BiScO$_3$-PbTiO$_3$.[1,2]

	25 °C				100 °C			
	E_C^p (E_C^s) (kV/cm)	E_C^p (E_C^s) deviation	P$_r$ (μC/cm^2)	d$_{33}$ (pC/N)	E_C^p (E_C^s) (kV/cm)	E_C^p (E_C^s) deviation	P$_r$ (μC/cm^2)	d$_{33}$ (pC/N)
Undoped	19.25 (17.61)	1.295 (2.93)	21.7	335	13.95 (11.61)	0.455 (0.495)	27.2	470
Doped	20.33 (18.62)	0.825 (1.475)	30	430	14.25 (12.59)	0.295 (0.295)	32.9	470

[1] E_C^p and E_C^s correspond to average Coercive field measured from ferroelectric loops and piezoelectric loops, respectively. Deviation values are the difference between the measured values and the average for coercive field.

[2] d$_{33}$ values are approximated from the ratio of maximum strain to maximum field at unipolar 40kV/cm.

Despite the lack of dependence of E$_c$ on composition, remanant polarization (P$_r$) was higher for the doped composition at room temperature (21.7μC/cm^2 and 27.2μC/cm^2 for undoped and doped specimens, respectively). Remenant polarization showed a more significant dependence on temperature for the undoped specimen and at 100°C P$_r$ was closer for both compositions; 30μC/cm^2 and 32.9μC/cm^2 for undoped and doped compositions, respectively. Dipolar polarizability of a dielectric shows the greatest temperature dependence and the increase of P$_r$ and P$_{max}$ for the undoped specimen can be related to an increase in dipolar polarizability or thoroughness of poling. Piezoelectrics with greater domain wall mobility can be poled more thoroughly even at lower temperatures. Therefore the thermal contribution to the polarization would decrease. However, for the systems with pinned domains, domain mobility has a larger dependence on the temperature.

The high temperature piezoelectric coefficients of the doped specimen were higher than the undoped specimen. Figure 26 shows the unipolar induced strain for both compositions at room temperature and at 100°C. The high field d$_{33}$ calculated as an
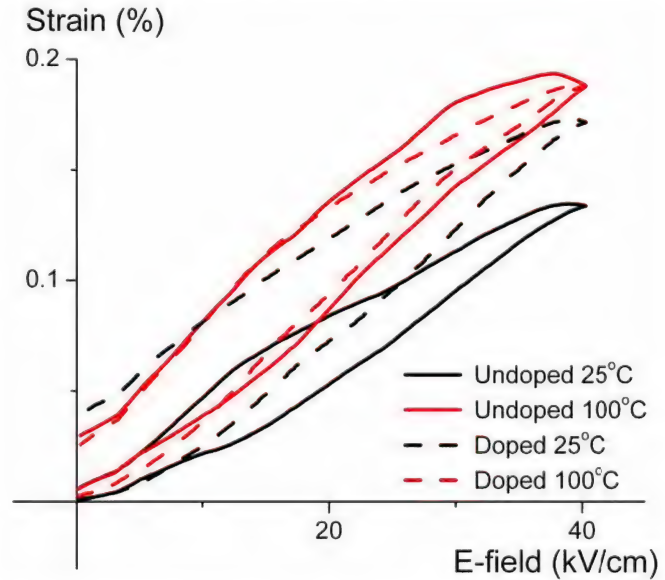

Fig. 26: Unipolar strain measurements as a function of electric field at room temperature and at 100 ^{o}C for both undoped and doped compositions.

approximation from the ratio of maximum strain to maximum field at 40kV/cm is given in Table VII for both temperatures. Doping increased the piezoelectric coefficient from ≈335pC/N to ≈430pC/N at room temperature. The high field piezoelectric coefficients were the same (≈470pC/N) for both undoped and doped compositions at 100°C.

Figure 27 shows the high field dielectric constants at DC-bias up to 40kV/cm. The high field was applied in a step-like fashion. The capacitance and tan δ measurement were conducted with an overlaying ac-signal of a magnitude of 5V and frequency of 1kHz. 5V approximately corresponds to 0.05kV/cm. The zero DC-field dielectric constants as measured by aixACCT and Agilent 4294A at room temperature and 100°C are summarized in Table VI. Despite variations in values between different measurement techniques, the dependence on composition was similar; increased dielectric constant for the doped composition. Dielectric constants decreased as the field increased. Similar to ferroelectric and piezoelectric loops, these bipolar measurements also showed asymmetry at low temperatures. The dielectric constant at 40kV/cm for doped and undoped specimens was similar both at room temperature and 100°C showing a larger change in the doped compositions as a function of electric field. At room temperature the change in dielectric constant upon application of an electric field (40kV/cm) was 23.6% and 33.6% for undoped and doped compositions, respectively; consistent with presence of more mobile domain walls in doped speci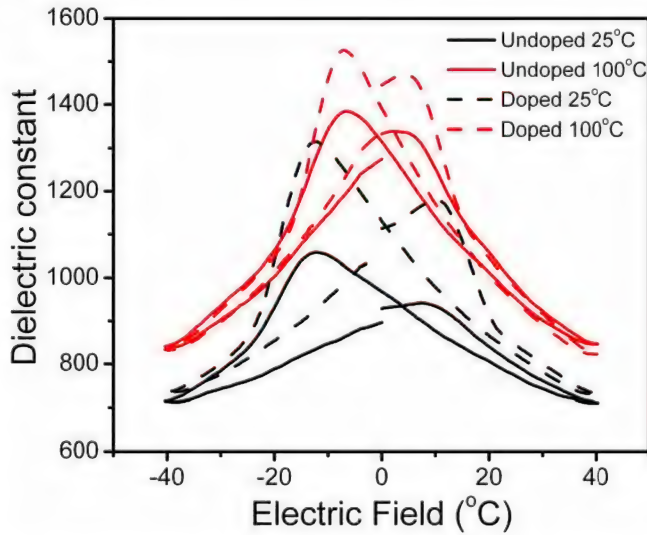mens. At 100°C the percentage drop in dielectric constant as a function electric field increased as expected for thermally activated domain walls. The decrease was 36.7% and 42.4% for the undoped and doped compositions, respectively. The difference between the behaviors of both compositions decreased at higher temperatures in a similar fashion to observations by other high field measurements (Fig 25 and 26). For all compositions at room temperature and at 100°C, tan δ was similar in value (≈0.09), higher than measurements by Agilent 4294A (Table VI). However, the lack of

Fig. 27: High field dielectric constant measurements as a function of electric field at room temperature and at 100 °C for both undoped and doped compositions.

dependence of tan δ on composition was consistent in both measurement conditions. At high fields tan δ decreased approximately down to ≈0.06, a ≈30% change.

Domain pinning would result in increased temperature dependence of polarization (Fig. 25) and decreased dielectric constant (Fig. 23), polarization (Fig. 25), piezoelectric coefficient (Fig. 26) and hysteresis in unipolar strain (Fig. 26), all of which are observed for undoped specimens. A-site vacancies enhance domain boundary motion that results in decreased coercive field, decreased temperature dependence and square hysteresis loops. Therefore doped composition is expected to have greater number of A-site vacancies. This contradicts the possibility of Pb filling the Bi-sites in the lattice. The change in properties however might be dominated by other factors such as the phase structure. Doped composition has lower concentration of tetragonal domains which has lower tetragonality as well (Table V). Such changes in the structure are expected to promote domain rotation and result in increased dielectric constant, polarization and hysteresis in unipolar strain, all of which are consistent with the measurements. The lack of dependence of E_c on composition also indicates the difficulty of explaining all the observation with discussion of singular effects. High field properties for both composition is similar to each other at 100°C (Figs. 25 and 26) indicating that thermally assisted domain motion eliminated the dependence of the domain wall mobility on the extrinsic contributions (i.e., defect structure induced by doping). However, weak field properties such as k_p and d_{31} still showed a dependence on composition at high temperatures.

High field DC-resistivity of both compositions was similar. Figure 28 shows the DC-resistivity of both specimens at 100 °C up to 50 kV/cm. For undoped specimens the resistivity exhibited an increase with increasing field. This increase was relatively insignificant, especially for the undoped compositions. Such an increase can be related to polarization rotation under DC-bias. When a sample is poled, upon removal of the field some dipoles re-orient resulting in a decrease in polarization. Consistent with the other measurements, the greater
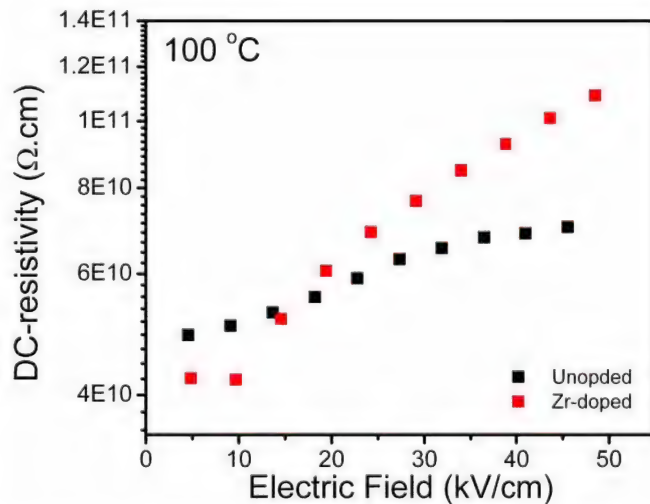

Fig. 28: DC-resistivity measurements as a function of temperature at 100 °C for both undoped and doped compositions.

increase observed for doped specimens indicate increased domain mobility. Figure 28 shows an inflection point in the resistivity data for both compositions just above E_c, implying the contribution of polarization rotation to the measured DC-resistivity. However, the magnitude of the change is small due to the square nature of the hysteresis loops (Figure 25).

III.   References:

1. B. Kiel, "Review of Advances in Combustion Control, Actuation, Sensing, Modeling and Related Technologies for Air Breathing Gas Turbines", AIAA Paper No. AIAA 2001-0481, presented at the AIAA 39th Aerospace Sciences Meeting, Reno, NV, Jan. 8-11, 2001

2. R.E. Eitel, C.A. Randall, T.R. Shrout, P.W. Rehrig, W. Hackenberger, and S.E. Park, "New High Temperature Morphotropic Phase Boundary Piezoelectrics Based on $Bi(Me)O_3$-$PbTiO_3$ Ceramics," Jpn. J. Appl. Phys. Pt. 1, **40** [10] 5999-6002 (2001).

3. R.E Eitel, C.A. Randall, T.R. Shrout, and S.E. Park, " Preparation and Characterization of High Temperature Perovskite Ferroelectrics in the Solid Solution $(1-x)BiScO_3$-$xPbTiO_3$," Jpn. J. Appl. Phys. Pt. 1, **41** [4A] 1999-2104 (2002).

4. Y. Inaguma, A. Miyaguchi, M. Yoshida, T. Katsumata, Y. Shimojo, R. Wang, and T. Sekiya, "High-Pressure Synthesis and Ferroelectric Properties in Perovskite-Type $BiScO_3$-$PbTiO_3$ Solid Solution," J. Appl. Phys., **95** [1] 231-235 (2004).

5. J. Iniguez, D. Vanderbilt, and L. Bellaiche, "First-Principles Study of $(BiScO_3)_{1-x}$-$(PbTiO_3)_x$ Piezoelectric Alloys," Phys. Rev. B, **67** [22] 224107 (2003).

6. S. Zhang, L. Lebrun, S. Rhee, R.E. Eitel, C.A. Randall, and T.R. Shrout, "Crystal Growth and Characterization of New High Curie Temperature $(1-x)BiScO_3$-$xPbTiO_3$ Single Crystals," J. Cryst. Growth, **236** 210-216 (2002).

7. S. Zhang, C.A. Randall, and T.R. Shrout, "Dielectric and Piezoelectric Properties of $BiScO_3$-$PbTiO_3$ Crystals with Morphotropic Phase Boundary Composition," Jpn. J. Appl. Phys., **43** [9A] 6199-6203 (2004).

8. S. Zhang, C.A. Randall, and T.R. Shrout, "High Curie Temperature Piezocrystals in the $BiScO_3$-$PbTiO_3$ Perovskite System," Appl. Phys. Lett., **83** [15] 3150-3152 (2003).

9. S. Zhang, C.A. Randall, and T.R. Shrout, "Characterization of Perovskite Piezoelectric Single Crystals of $0.43BiScO_3$-$0.57PbTiO_3$ with High Curie Temperature," J. Appl. Phys., **95** [8] 4291-4295 (2004).

10. S. Zhang, C.A. Randall, and T.R. Shrout, "Dielectric, Piezoelectric, and Elastic Properties of Tetragonal $BiScO_3$-$PbTiO_3$ Single Crystal with Single Domain," Solid State Commun., **131** 41-45 (2004).

11. S. Zhang, C.A. Randall, and T.R. Shrout, "Recent Developments in High Curie Temperature Perovskite Single Crystals," IEEE Trans. Ultrason. Ferroelectr. Freq. Control, **52** [4] 564-569 (2005).

12. R.E. Eitel, S.J. Zhang, T.R. Shrout, C.A. Randall, and I. Levin, "Phase Diagram of Perovskite System $(1-x)BiScO_3$-$xPbTiO_3$," J. Appl. Phys., **96** [5] 2828-2831 (2004).

13. C.A. Randall, R.E. Eitel, T.R. Shrout, D.I. Woodward and I.M. Reaney, "Transmission Electron Microscopy Investigation of the High Temperature $BiScO_3$-$PbTiO_3$ Piezoelectric Ceramic System," J. Appl. Phys., **93** [11] 9271-9274 (2003).

14. I. Grinberg, M.R. Suchomel, P.K. Davies, and A.M. Rappe, "Predicting Morphotropic Phase Boundary Locations and Transition Temperatures in Pb- and Bi-based Perovskite Solid Solutions from Crystal Chemical Data and First-Principles Calculations," J. Appl. Phys., **98** [9] 094111 (2005).

15. M.R. Suchomel, and P.K. Davies, "Predicting the Position of the Morphotropic Phase Boundary in High Temperature $PbTiO_3$-Bi(B'B'')O_3 Based Dielectric Ceramics," J. Appl. Phys., **96** [8] 4405-4410 (2004).

16. J. Cheng, R.E. Eitel, N. Li, and L.E. Cross, "Structural and Electrical Properties of (1-x)Bi($Ga_{1/4}Sc_{3/4}$)O_3-$xPbTiO_3$ Piezoelectric Ceramics," J. Appl. Phys., **94** [1] 605-609 (2003).

17. R.E. Eitel, T.R. Shrout, and C.A. Randall, "Tailoring Properties and Performance of (1-x)$BiScO_3$-$xPbTiO_3$ Based Piezoceramics by Lanthanum Substitution," Jpn. J. Appl. Phys., **43** [12] 8146-8150 (2004).

18. P. Winotai, N. Udomkan, and S. Meejoo, "Piezoelectric Properties of Fe_2O_3-doped (1-x)$BiScO_3$-$xPbTiO_3$ Ceramics," Sensor. Actua. A, **122** 257-263 (2005).

19. I. Sterianou, I.M. Reaney, D.C. Sinclair, D.I. Woodward, D.A. Hall, A.J. Bell, and T.P. Comyn, "High Temperature (1-x)$BiSc_{1/2}Fe_{1/2}O3$-$xPbTiO_3$ Piezoelectric Ceramics," Appl. Phys. Lett., **87** [24] 242901 3pp. (2005).

20. S. Chen, X. Dong, H. Yang, R. Liang, and C. Mao, "Effects of Niobium Doping on the Microstructure and Electrical Properties of 0.36$BiScO_3$-0.64$PbTiO_3$ Ceramics," J. Am. Ceram. Soc., **90** [2] 477-482 (2007).

21. S. Zhang, E.F. Alberta, R.E. Eitel, C.A. Randall, and T.R. Shrout, "Elastic, Piezoelectric, and Dielectric Characterization of Modified $BiScO_3$-$PbTiO_3$ Ceramics," IEEE Trans. Ultrason. Ferroelectr. Freq. Control, **52** [11] 2131-2139 (2005).

22. S. Zhang, R.E. Eitel, C.A. Randall, T.R. Shrout, and E.F. Alberta, "Mangenese-Modified $BiScO_3$-$PbTiO_3$ Piezoelectric Ceramic for High-Temperature Shear mode Sensor," Appl. Phys. Lett., **86** [26] 262904 3pp. (2005).

23. M.N. Rahaman, Ceramics Processing and Sintering, Marcel Dekker Inc., New York, NY, pp. 520-521 (1995).

24. D. Kobor, B. Guiffard, L. Leburn, A. Hajjaji, and D. Guyomar, "Oxygen Vacancies Effect on Ionic Conductivity and Relaxation Phenomenon in Undoped and Mn Doped PZN-4.5PT Single Crystals," J. Phys. D: Appl. Phys., **40** 2920-2926 (2007).

25. A.R. James, S. Priya, K. Uchino, K. Srinivas, and V.V. Kiran, "Investigations of Intrinsic Defect Structure in 0.91Pb($Zn_{1/3}Nb_{2/3}$)O_3-0.09$PbTiO_3$ Single Crystal through AC Conductivity," Jpn. J. Appl. Phys., **41** [8] 5272-5276 (2002).

26. B. Jaffe, W.R. Cook, and H. Jaffe, Piezoelectric Ceramics, Academic Press Limited, London, pp.135-147 & 154-158 (1971).

27. A.J. Moulson, and J.M. Herbert, Electroceramics: Materials, Properties, Applications, Chapman&Hall, London, pp. 61 (1997).

28. J.R. Macdonald, Impedance Spectroscopy: Emphasizing Solid Materials and Systems, John Wiley & Sons, New York, NY, pp. 6-7 and 217-225 (1987).

29. ANSI/IEEE 176-1987, IEEE Standard on Piezoelectricity, IEEE, New York (1987).

IV. Publications and Presentations:

Journal papers:

A. Sehirlioglu, A. Sayir, F. Dynys, Krishna Nittala, and Jacob Jones, "Exploration of $BiScO_3$-$PbZrO_3$-$PbTiO_3$ Ternary for Enhanced Piezoelectrics, Part I: Structure and Phase Transformations" *in preparation*, J. Am. Ceram. Soc., 2009.

A. Sehirlioglu, A. Sayir, F. Dynys, Krishna Nittala, and Jacob Jones, "Exploration of $BiScO_3$-$PbZrO_3$-$PbTiO_3$ Ternary for Enhanced Piezoelectrics, Part II: Electrical and Electromechanical Properties" *in preparation*, J. Am. Ceram. Soc., 2009.

A. Sehirlioglu, A. Sayir, and F. Dynys, "Enhanced Ferroelectric and Electromechanical Properties of Doped $BiScO_3$-$PbTiO_3$ Ceramics", *in preparation,* J. Appl. Phys., 2009

A. Sehirlioglu, A. Sayir, and F. Dynys, "High Temperature Properties of $BiScO_3$-$PbTiO_3$ Ferroelectric Ceramics," *submitted to* J. Appl. Phys., 2009.

A. Sehirlioglu, A. Sayir, and F. Dynys, "Microstructure-Property Relationships in Liquid Phase Sintered High-Temperature Bismuth Scandium Oxide-Lead Titanate Piezoceramics," J. Am. Ceram. Soc., **91** [9], 2910 (2008).

Invited seminars:

A. Sehirlioglu, A. Sayir, F. Dynys, D.A Payne, and P.D. Han, Department Colloquium, Case Western Reserve University, Cleveland, OH, Jan 2009.

A. Sehirlioglu, A. Sayir, and F. Dynys, Florida University, Ganiesville, FL, Apr 2008.

A. Sehirlioglu, A. Sayir, and F. Dynys, University of Central Florida, Orlando, FL, Apr 2008.

A. Sehirlioglu, A. Sayir, F. Dynys, D.A Payne, and P.D. Han, Sandia National Laboratories, Albuquerque, NM, Feb 2008.

A. Sehirlioglu, A. Sayir, F. Dynys, D.A Payne, and P.D. Han, Alfred University, Alfred, NY, Feb 2008.

Invited presentations:

A.Sehirlioglu, A. Sayir, and F. Dynys, "Exploring the BiScO3-PbTiO3-PbZrO3 Ternary for Enhanced High Temperature Piezoceramics," U.S. Navy Workshop on Acoustic Transduction Materials and Devices, State College, PA (2009).

A.Sehirlioglu, A. Sayir, and F. Dynys "Effects of Excess Bi and Pb on the Electrical Properties of BiScO3-PbTiO3 ceramics," Invited talk at the Materials Science and Technology meeting, Detroit, MI (2007).

Presentations:

A. Sehirlioglu, A. Sayir and F. Dynys, "Enhanced High Temperature Piezoelectrics Based on $BiScO_3$-$PbTiO_3$ Ceramics," 33th International Conference and Exposition on Advanced Ceramics and Composites, Daytona Beach, FL (2009).

A. Sehirlioglu, A. Sayir and F. Dynys, "Effect of excess PbO and Bi_2O_3 content on the electrical properties of high-temperature $BiScO_3$-$PbTiO_3$ ceramics," 17th IEEE International Conference on Applications of Ferroelectrics, Santa Fe, NM, US (2008).

A. Sehirlioglu, A. Sayir and F. Dynys, "Doping of $BiScO_3$-$PbTiO_3$ Ceramics for Enhanced Properties," Materials Science and Technology meeting, Pittsburgh, PA (2008).

A.Sehirlioglu, and A. Sayir, "High temperature piezoelectrics," Workshop on Ultra-High Temperature Ceramics, San Francisco, CA (2007).